Tailoring Cation Exchange in Nanomaterials

Katarina Condric
Master Thesis

Tailoring Cation Exchange in Nanomaterials

Master Thesis

Katarina Condric

Supervisors:
Celso de Mello Donegá
Serena Busatto & Raimon Terricabres-Polo
Utrecht University
Condensed Matter & Interfaces
December 2022

Abstract

In this thesis, metal exchange in two different nanocrystalline systems is explored. Firstly, the partial In^{3+} for Cu^{+} cation exchange in a colloidal nanocrystal system of copper sulfide is studied. Excess trioctylphosphine is determined to be an effective addition to the cation exchange reaction that stabilizes the resulting wurtzite copper indium sulfide nanocrystals and allows for samples synthesized with less than stoichiometric In/Cu precursor ratios to be luminescent. Additionally, gallium incorporation into these $CuInS_2$ nanocrystals is shown to improve and blue shift the luminescence.

Secondly, cadmium for indium exchange is studied in a solid system of InSb nanowires. This reaction is unexpected due to the covalent character of the initial material. However, the reaction is discovered to undergo complete transformation from InSb to Cd_3Sb_2 upon reaction of a nanowire wafer with a cadmium oleate solution containing an excess of oleic acid. This complete transformation does not occur with other metal oleates, such as, copper, zinc and bismuth, in the same manner, or at all.

Cation exchange is observed, and the progress monitored in colloidal nanocrystal systems and solid templates. Studying these cation exchanges helps us to understand the mechanisms of the reactions and predict the outcomes of similar exchange systems.

Contents

1. Introduction

The idea behind this project is to investigate cation exchange in two completely different sources of templates. A colloidal nanocrystal system, which should be unaffected by the limitations of solid-state diffusion, and an attached nanowire system containing much larger nanostructures. Each system consists of aliovalent atoms to be exchanged. Colloidal $CuInS_2$ nanocrystals are stabilized in solution by ligands whereas the InSb nanostructures are bare, with a well-defined surface.

This thesis explores detailed manipulation of variables in two examples of metal exchange. The first part delves into why cation exchange is chosen and its advantages over direct synthesis. In chapter 3, the exploration of copper indium sulfide ($CuInS_2$) nanocrystals and their synthesis and characterization are detailed. Finally, the transformation of InSb nanowires to Cd_3Sb_2 is explored in chapter 4 and a mechanism of the reaction is proposed.

Investigating the intricate details of both of these systems allows us to better understand the mechanisms of exchange and the requirements of the reaction to proceed to completion.

2. Theory and Background

2.1 Nanomaterials

Nanomaterials are the hot new topic, but why is understanding them so important? Bonding in small metal or semiconductor clusters varies from the bulk, and the behaviour of an atom at the surface differs from one inside a cluster. In the case of a spherical particle, the surface area scales with the radius squared, r^2, while the volume scales with r^3.[1] Thus, as the radius of the particle becomes increasingly smaller, the surface area will be much larger than the volume, leading to a large surface area to volume ratio. The number of atoms at the surface of the particles, scales with this ratio. The decreasing size of particles leads to quantum confinement.[2] We see discontinuous behaviour due to the completion of shells in systems with delocalized electrons. Atoms have well defined orbitals. These orbitals can be combined to extended band structures and and the position of the fermi level determines whether the material is a metal or an insulator. The core orbitals are confined to a small volume and remain localized. Each atom contributes to a band with its atomic states such that the width of the band increases when more atoms are added. The density of states within a band is proportional to the number of atoms in the ensemble of the extended and structure. This means that the density of states scales with size. This can be represented by the particle in the box model, such that the size of the box is proportional to the size of the particle.[1]

2.2 Semiconductors

The properties of a material are determined by the electrons in the material. If there is no confinement, the material is free to absorb energy of any magnitude.[3,4] When there is confinement, a material is limited to absorbing energy equal to or greater than the energy gap of the material. A semiconductor is a material that has a full valence band and an empty conduction band. When an electron is promoted from the valence band to the conduction band, for example by means of photon absorption of energy ≥ the energy gap between the two bands, this promotion creates charge carriers in each band.[2] A hole in the valence band and an electron in the conduction band. This electron/hole pair forms an exciton. [2,3]

2.2.1 Semiconductor nanocrystals

In a semiconductor nanocrystal, the valence and conduction band are not as in the bulk, but instead contain discrete energy levels at the edges of the bands (Figure 2.1). Additionally, shown in Figure 2.1, due to quantum confinement, the smaller the particle, stronger confinement and so, the larger the gap between these two bands. This gap is analogous to the HOMO-LUMO gap in molecules. The size of the particle can thus be used to tune the size of the bandgap.[2,3]

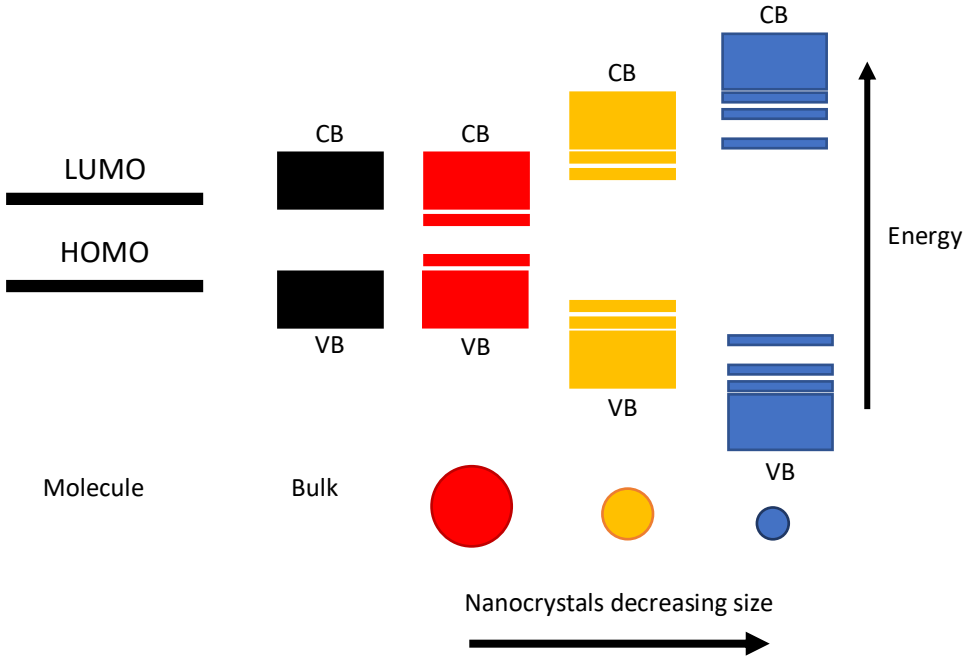

Figure 2. 1: *Graphic representation of HOMO and LUMO or conduction (CB) and valence (VB) bands in bulk and nanocrystals demonstrating confinement effects. Adapted from [2]*

The exciton created by the electron/hole pair can decay in a few manners, including radiative and non-radiative decay. Radiative decay results in the emission of a photon and non-radiative decay can result in, for example, vibrations.[2]

As energy is inversely proportional to the wavelength, reflected in the equation for the energy of a photon in equation (1), this means that the smallest quantum dots will emit violet photons, and the largest, red.

$$E = \frac{hc}{\lambda} \quad (1)$$

The size and the shape of semiconductor nanocrystals is dictated by the synthesis and the limitations of the synthetic method.[2,3] Colloidal synthetic methods of nanomaterials include hot injection, dropwise addition, alternate addition, seeded injection, and cation exchange. In this work, colloidal hot injection synthesis is used and post synthetic modification of the nanomaterials is carried out by metal/cation exchange.

2.3 Post synthetic modification of nanomaterials

It is often useful to tune the physical properties of materials such that the performance of the material can be adjusted. These physical properties include but are not limited to, size,

shape, composition, structure, and morphology. Post synthetic modification of materials at the macro and nanoscale can proceed by one of several methods. The methods discussed in this work are cation exchange and galvanic replacement.

2.3.1 Cation exchange

The first method, and the focus of this thesis, is cation exchange. As mentioned before, physical and chemical properties of materials change as these materials are brought to the nanoscale. Nanomaterials are commonly synthesized by hot injection. In this method, the precursors are decomposed due to the high temperature and induce a burst of nucleation, which is followed by uniform growth of particles. However, this hot injection method requires a thorough understanding and balance of the nucleation, and growth of the particles, as well as the surface kinetics[6].

Ion exchange is a popular tool, because it can be used to substitute ions in a solid for those in solution and is a common processing technique for thin film semi-conductors. The use of ion exchange, especially cation exchange, at the nanoscale is beneficial because it allows for the retention of shape and morphology, and the reaction is fast because there is little solid-state diffusion that must be overcome, due to the large surface area to volume ratio of the nanoparticles. Conversely, anion exchange is possible,[6] which ion is exchanged is usually dictated by which ion is smaller in the framework of the crystal.

2.3.2 Galvanic replacement

The second method that may be used to convert materials is galvanic replacement. Galvanic replacement is an electrochemical process in which one metal is oxidized by another metal that has a higher reduction potential.[5,7] In a solution, the template metal is oxidized while the second is reduced. The first metal is dissolved into solution and the second is plated onto the template. In other words, the template metal is corroded, and this reaction can be represented by the two half reactions below. In equation (2), an oxidation occurs as the zinc metal loses electrons. These electrons are consequently used for the reduction of copper as the ion accepts the electrons to become copper metal, equation (3).

$$Zn_{(s)} \rightarrow Zn^{2+} + 2e^{-} \quad (2)$$

$$Cu^{2+} + 2e^{-} \rightarrow Cu_{(s)} \quad (3)$$

For the reaction to succeed, the reduction potential of the second metal must be sufficiently higher than the first. In the case of zinc and copper, their reduction potentials with respect to a standard hydrogen electrode, are - 0.762 eV and 0.339 eV.[8] The reduction potential of copper is therefore much higher and thus the reaction will proceed spontaneously. As this is the driving force, it can be said that the only limitation of this method is that the difference between the reduction potentials must be high enough to be favoured in the direction of the reduction half reaction.

The spatial distribution of ions in the final material can also be dictated by the order of precursor addition in the reaction[3]. This makes it possible for hollow structures to be created. The oxidation creates lattice vacancies, which aggregate together to reduce surface free energy. These holes aggregating together can be used to the advantage of the synthesis, to make hollow structures.[5,7]

At the macro scale, galvanic replacement is well understood and can be observed with the naked eye. Additionally, this method is used daily for applications such as batteries,

anticorrosion, plating, and can also be used for decorative plating.[5,9] In nanomaterials, the process is also possible, but more difficult to track.

Galvanic replacement is an attractive method for transforming materials because it is not specific to size, shape, or material, and thus should be effective for any material if the difference between reduction potentials of the two metals is sufficient.[5] It is important to note that the shape of the original material is not preserved through galvanic replacement.

2.4 Applications

Below is a quick overview of some of the potential applications of the metal/cation exchanged nanomaterials synthesized in this work.

2.4.1 Applications of $CuInS_2$ nanocrystals

Luminescent solar concentrators are devices that were proposed in the 1970's. These devices trap light that is then to be connected to photovoltaic cells.[10] The basic model is a rectangle of a transparent material such as PMMA in which absorbers are embedded. These absorbers, historically organic dyes, absorbs light in the visible or UV range and then emit photons. These emitted photons are trapped by total internal reflection and these reflections guide the photons to the edges of the device where photovoltaic cells are mounted.[10,11] It is worth noting that these devices do not need to be coupled with photovoltaic cells, they can be used for example, to simply generate light,[12] (but coupling with photovoltaic cells is a common application, in the ever present effort to make the world more sustainable. These devices are still studied, but they are poorly efficient, typically in the range of 4%, [12,13] whether due to radiative losses such as, Stokes-shift energy loss, self-absorption, and reabsorption or non-radiative losses such as, quenching or host scattering and reabsorption.[11,13] A potential alternative to organic dyes that were originally used, could be quantum dots. Quantum dots have broader absorption bands, that can go well into the UV range, and their absorbance can be tuned by the size of the particles. These quantum dots are also more stable than organic dyes.[13]

2.4.2 Applications of InSb nanowires and CdSb

InSb nanowires semiconductors with a small bandgap and are proposed for use in quantum computing. This material has a high electron mobility and strong spin orbit coupling. These properties of the nanowires allow for the generation of a topological superconducting region in the wires where Majorana fermions can appear. These Majorana fermions are the basis for the quantum computing.[14,15,16] CdSb is also a material with a narrow bandgap, high electron mobility and it also has low thermal conductivity which makes it a promising thermoelectric material. It is not possible to synthesize nanowires of this material from scratch and so it may be used to coat existing nanowires of other compositions to improve its electronic properties.[17]

2.7 References

[1] Roduner, E. Size Matters: Why Nanomaterials are Different. *Chem. Soc. Rev.* 35, 583-592, (2006)

[2] Koole, R., Groeneveld, E., Vanmaekelbergh, D., Meijerink, A. & de Mello Donega, C. in *Nanoparti- cles: Workhorses of Nanoscience* (Springer-Verlag, 2015).

[3] El Sayed, M.A., Small Is Different: Shape-, Size-, and Composition-Dependent Properties of Some Colloidal Semiconductor Nanocrystals. *Acc. Chem. Res.* 37(5), 326–333, (2004).

[4] Lukasiak, L., Jakubowski, A. History of Semiconductors. *J. Telecommun. Inf. Technol.* 1(2010).

[5] Xia, X., Wang, Y., Ruditskiy, A., Xia, Y. Galvanic Replacement: A Simple and Versatile Route to Hollow Nanostructures with Tunable and Well-Controlled Properties. *Adv. Mater.* 25(44), 6316-6333 (2013).

[6] Beberwyck, B.J., Surendranath, Y., Alivisatos, A.P. Cation Exchange: A Versatile Tool for Nanomaterial Synthesis. *J. Phys. Chem. C.* 117, 19759-19770, (2013)

[7] Oh, MH., et al. Galvanic Replacement Reactions in Metal Oxide Nanocrystals. *Science.* 340(6135), 964-968, (2013).

[8] Harris, D. C. (2010). *Quantitative Chemical Analysis, 8th Edition*. W.H. Freeman.

[9] Papaderakis, A., et al. Electrocatalysts Prepared by Galvanic Replacement. *Catalysts.* 7(3), 80, (2017).

[10] Batchelder, J.S., Zewail, A.H., Cole, T. Luminescent Solar Concentrators. 1: Theory of Operation and Techniques for Performance Evaluation. *Appl. Opt.* 18(18), 3090-3110, (1979).

[11] Hermann, A.M. Luminescent Solar Concentrators – A Review. *Sol. Energy*. 29(4), 323-329, (1982).

[12] Papakonstantinou, I., Portnoi, M., Debije, M.G. The Hidden Potential of Luminescent Solar Concentrators. *Adv. Energy Mater.* 11, 2002883, (2021).

[13] van Sark, W.G.J.H.M., et al. Luminescent Solar Concentrators – A Review of Recent Results. *Opt. Express.* 16(26), 21773-21792, (2008).

[14]Badawy, G., et al. High Mobility Stemless InSb Nanowires. *Nano Lett.* 19, 3575-3582, (2019).

[15] Park, H. D., et al. Growth of high quality, epitaxial InSb nanowires. *J. Cryst. Growth.* 304, 2, 399-401, (2007).

[16] van Weperen, I., et al. Quantized Conductance in an InSb Nanowire, *Nano Lett.* 13, 2, 387–391, (2013)

[17] wang, S., et al. Anisotropic Multicenter Bonding and High Thermoelectric Performance in Electron-Poor CdSb. *Chem. Mater.* 27, 3, 1071–1081, (2015).

3. Tailoring cation exchange in $CuInS_2$ nanocrystals

3.1 Introduction

Copper indium sulfide, $CuInS_2$, nanocrystals (NCs) are commonly used semiconductor nanoparticles sometimes also called quantum dots. $CuInS_2$ NCs can adopt one of two crystal structures, wurtzite, or chalcopyrite.[1,2,3] The crystal structure is important to consider because it greatly dictates the optical properties of the material. Chalcopyrite $CuInS_2$ has a band gap of 1.5 eV,[1] while wurtzite $CuInS_2$ has a bandgap of 1.3 eV,[4] and is therefore, both are a good candidate for use in photovoltaics.[5] These NCs are of particular interest for use in the aforementioned luminescent solar concentrators due to their tuneable NIR emission.[6]

There is a significant amount of work investigating the chalcopyrite $CuInS_2$ NCs, and limited investigation into the wurtzite $CuInS_2$ NCs, their optimization of their will be discussed in this section. Broadening our knowledge of these NCs allows for more potential to break into the market with novel materials. Additionally, the I-III-VI ternary semiconductor NCs can be tricky to synthesize because they require balancing of many precursors, thus, cation exchange is an effective tool to synthesize these NCs.[6]

Wurtzite $CuInS2_2$ NCs are synthesized by cation exchange using template $Cu_{2-x}S$ NCs where $0 \leq x \leq 1$. The vacancies in the framework allow for oscillations and induce surface plasmon resonance. Varying the number of vacancies in the framework, changes the position of the plasmon resonance. The presence of these vacancies allows for variation of the crystal structure and the stoichiometry.[6] Published works for the synthesis of wurtzite $CuInS_2$ NCs were found to be poorly reproducible at the reduced scale that was needed to test many variables and investigate how each variable affects the resulting luminescent $CuInS_2$ NCs. Varied In/Cu ratios were explored, as well as the effect of addition of extra trioctlyphosphine into the reaction.

Ga^{3+} incorporation into chalcopyrite $CuInS_2$ NCs has been proven to improve luminescence in these particles.[7] This is carried out by using complexed $GaCl_3$, (with a phosphine ligand, DPP or DDT) to prevent the etching of the particles, and to allow for Ga^{3+} incorporation, as Cu^+ is extracted from the NCs. This method is explored in this work to see if it is also an effective tool to be used to increase luminescence in wurtzite type $CuInS_2$ NCs as well.

The goal of this project is to improve the synthesis and optical properties of such NCs that are proposed for use in luminescent solar concentrators. However, only the synthesis and characterization of these NCs are discussed, therefore, a deeper discussion of the working principles of luminescent solar concentrators is beyond the scope of this thesis.

3.2 Experimental

3.2.1 Chemicals

Copper (I) acetate (Cu(OAc), Sigma-Aldrich, 97%), Indium (III) chloride ($InCl_3$, Sigma Aldrich, 98%), 1-dodecanethiol (DDT, Sigma Aldrich, ≥99.8%, degassed), 1-Octadecene (ODE, Thermo Scientific, 90% technical, degassed), Trioctylphosphine oxide (TOPO, Sigma Aldrich, 99%), Trioctylphosphine (TOP, Sigma-Aldrich, 90%), Octylamine (Sigma Aldrich, 99%), Toluene (Alfa Aesar, anhydrous, 99.8%), Methanol (MeOH, Thermo-

Scientific, ≥99.9%), 1-Butanol (BuOH, Sigma-Aldrich, anhydrous, 99.8%), Gallium chloride ($GaCl_3$, Alfa Aesar, 99.99%), Diphenylphosphine (DPP, Sigma-Aldrich, 98%), Indium acetate ($In(OAc)_3$, Sigma-Aldrich, 99.99%).

Degassing of chemicals such as DDT and ODE, done by applying vacuum at 120 °C for 2 hours.

3.2.2 Synthesis

Except where noted otherwise, all reactions and washing steps were carried out in a glovebox under nitrogen atmosphere, $[O_2] \leq 3$ ppm and $[H_2O] = 0$ ppm. All chemicals used are anhydrous or degassed.

3.2.2.a Synthesis of $Cu_{2-x}S$ template nanocrystals

The synthesis procedure is adapted from a protocol published by Xia et al.[2] A batch of template NCs was synthesized for use in many consequent cation exchange reactions. In the synthesis, 1.0 mmol (0.126 g) copper (I) acetate, 4.65 mmol (1.834 g) of TOPO and 10 mL of ODE were degassed in a Schlenk line for 1 hour at 100 ºC. This resulted in an opaque dark green/yellow solution. Upon degassing, the reaction vessel was filled with nitrogen, and the temperature was set to 210 ºC. As the solution heated, at 160 ºC, 10.85 mmol (2.6 mL) of DDT was injected into the solution. Upon injection there was a colour change sequentially from green to orange, to red, and to brown. Once the solution reached 210 ºC, the reaction was allowed to progress for 30 mins. The vessel was then taken off the heat and cooled to room temperature naturally before washing.

For the first washing, the solution was divided over two 40 mL glass vials, and 20 mL of an isometric mixture of MeOH and BuOH was added to each. This mixture was centrifuged at 1471 RCF (2750 RPM) for 15 minutes. The supernatant was discarded, the solid dried under vacuum, and the resulting NCs were resuspended in (total) 2 mL toluene and reunited in one 20 mL glass vial (~250 µL of the template in toluene is saved for optical measurements and electron microscopy). The washing procedure was repeated two more times. Resulting NCs were dried under vacuum and then redispersed in 5 mL each of DDT and ODE in that order. The mixture was sonicated well between the addition of solvents and before use in cation exchange to ensure a homogenous mixture.

3.2.2.b In^{3+} incorporation into $Cu_{2-x}S$ template nanocrystals

The synthesis of wurtzite $CuInS_2$ NCs by partial Cu^+ for In^{3+} exchange was adapted from the protocol published by Xia et al.[2] The cation exchange volume is scaled down such that many variables or In/Cu ratios can be probed with one set of templates. The basic procedure began with the preparation of an indium precursor. 1.0 mmol (0.221 g) of $InCl_3$ and an equimolar amount of TOP (500 µL) are added to 9.5 mL of ODE, to prepare a 100 mM solution. This volume can be scaled to the amount of precursor needed for reactions because the precursor does not need to be prepared fresh. This precursor solution was heated to 125 ºC for 1 hour until it became clear. The precursor solution is stored as is in a glove box, only to be heated before use in reaction to ensure homogeneity. For the cation exchange, a desired amount of precursor (dependent on the desired In/Cu ratio) was added to a volume of ODE, enough to bring the total reaction volume to 3 mL, and heated to 125 ºC. Once the solution reached this temperature, an aliquot, (0.5 mL) of the stock solution of template NCs was added and reaction

time began. For all In/Cu ratios and following TOP additions, the reaction proceeded for one hour and was then removed from heat and allowed to cool to room temperature.

To wash the $CuInS_2$ NCs, 0.5 mL toluene, 6 mL of the isometric MeOH/BuOH mixture and 150 µL of octylamine was added to each vial. This mixture was centrifuged for 15 min at 1471 RCF (2750 RPM), supernatant was discarded, and the solid is washed once more. The solid was dried under vacuum and then redispersed in 1-2 mL of toluene for measurements. Volume noted to ensure consistent concentration for optical measurements.

3.2.2.c Ga^{3+} incorporation into $CuInS_2$ nanocrystals

A proof of concept set of Ga^{3+} cation exchanges was carried out to ensure that the method works. Several Ga^{3+} precursors were prepared, with $GaCl_3$ as the Ga^{3+} source, and either DDT or DPP as the ligand, and toluene or ODE as the solvent.[7]

2.5 mmol (0.440 g) $GaCl_3$, 2.5 mmol of DDT (0.600 mL) or DPP (0.435 mL) were added to a vial and placed on a heating block to melt for 15 minutes, and then the chosen solvent was added to bring the solution volume to 5 mL. This precursor was heated to 100 ºC and then 0.25 mL of a suspension of the template $CuInS_2$ NCs in toluene were injected, and the reaction was carried out for 30 minutes. After reaction, the solution was removed from heat and allowed to cool to room temperature.

To wash these samples, isometric MeOH/BuOH was added until the solution became cloudy and then centrifuged at 1471 RCF (2750 RPM) for 15 minutes. The supernatant was discarded and resuspended in toluene. The NCs were washed two more times. Finally, the particles were resuspended in 0.5 mL toluene for optical measurements.

3.2.3 Characterization

Absorption spectra obtained using a Perkin Elmer Lambda 950 UV/VIS/NIR spectrophotometer. Luminescence measurements were recorded with an Edinburgh Instruments FLS920 spectrofluorimeter equipped with a 450 W Xe lamp, excitation monochromator blazed at 300 nm and emission monochromator blazed at 500 nm.

Transmission electron microscopy (TEM) images were taken with a Thermo Scientific Talos F200X transmission electron microscope, with an accelerating voltage of 200 kV. Scanning transmission electron microscopy (STEM), and high-angle annular dark-field imaging (HAADF) images were used to measure NC sizes. Typically, 200 NCs were measured by hand in the program FIJI after which the average and standard deviation were given. Energy dispersive X-ray spectroscopy (EDS) measurements were used for elemental analysis.

Samples were prepared for TEM analysis by drop-casting the dilute solution onto copper or gold (for elemental analysis) grids. Subsequently, the grids were dried and then cleaned by submerging in a vial containing 5 mL ethanol and some activated carbon. The grids are submerged in this solution until the bubbling of the solution subsides, and then dried in air.[8]

3.3 Results and discussion

In the following discussion, different variables and specific reaction conditions are explored to show how reproducible optimal conditions were uncovered for this reaction. It was quickly determined that the reproducibility of this synthesis was not consistent and thus the goal of this project was to find a way to improve the reproducibility of these luminescent NCs. The published procedures are all with a set ratio of In/Cu in the reactants and it was our goal

to see how far we could push the limits of this reaction, to determine if there is an set of reaction conditions that can produce sub-stoichiometric $CuInS_2$.

In/Cu molar ratios are assumed based on the postulation that the template $Cu_{2-x}S$ NC synthesis is quantitative and there are no losses. The indium content is known exactly from the amount added to the precursor, so the TOP/In ratios in the discussion are expressed in excess to the known indium.

3.3.1 $Cu_{2-x}S$ template nanocrystals

Several batches of template $Cu_{2-x}S$ NCs were synthesized for use in cation exchange experiments. Upon first inspection of the absorption spectra of these syntheses, there are evident differences between the templates (Figure 3.1). Additionally, the samples behaved differently when used for cation exchange experiments a deeper look at the template NCs was necessary. All samples were very cloudy, indicating aggregation and poor colloidal stability, which is also represented in the absorbance spectra in Figure 3.1. There is a staggering difference in the absorption spectra of templates $Cu_{2-x}S$ NCs #1 and #2-5, and this can be attributed to the use of a different heating mantle, which had a different heat ramping rate. Template $Cu_{2-x}S$ NCs #1 were synthesized using a template which a much greater heating rate, and the temperature dropped quite often. A heating mantle with a slower but more consistent heating rate was then used for template $Cu_{2-x}S$ NCs #2-5 to ensure constant heating rates. Apart from this difference, to the best of ability, all the template syntheses were carried out as similarly as possible, so it is difficult to pinpoint where the variance in the templates originates. Evidence that the heating rate affects the template synthesis is shown in Figure 3.2.A, where the templates are clearly not polyhedral as expected, but instead they are platelets. Additionally in Figure 3.3.A, these platelets self-assemble into large > 1 μm corn like arrays, and this aggregation is confirmed by the cloudiness of the solution. Despite the differences in the scattering contribution and plasmon resonance in sample template $Cu_{2-x}S$ NCs #3-5, there is a feature appearing at 489, 492 and 491 nm respectively in each spectrum. The position of these features is calculated using the minimum of the second derivative of the absorption spectrum, (these plots can be found in Figure A1.1). This feature originates from the amount of vacancies in the $Cu_{2-x}S$ NC. The consistent position of this shoulder indicates a consistent number of vacancies throughout the samples #3-5. The variability then originates from the size dispersion, and the position of the surface plasmon resonance peak. The surface plasmon resonance appears due to the free holes cause by copper deficiencies in the nanocrystals structure, and its position is somewhat dependent on the size of the NCs. The plasmon resonance is mostly masked by the scattering contribution of the NCs that is likely due to aggregation and self-organization of the NCs.[6]

From the images shown in Figures 3.2 and 3.3, each sample appears different, has a different size, and behaves differently in solution, as shown in the absorption spectra in Figure 3.1. Template $Cu_{2-x}S$ NCs #2 and #3, in Figures 3.2. and 3.3 B and C respectively, exhibit the most similar size and best colloidal dispersion behaviour, with template $Cu_{2-x}S$ NCs #2 showing smaller size dispersion. Template $Cu_{2-x}S$ NCs #4, in Figures 3.2 and 3.3 D, there is very evident aggregation showing very distinct alignment in the pattern, suggesting unstable particles. Upon looking at a lower magnification TEM image of template $Cu_{2-x}S$ NCs #5, in Figure 3.3.E, there appears to be left over organic matter, which appears to trap the

nanocrystals. This was not analysed in detail but it can be suggested that perhaps this is leftover Cu(DDT). This template does not disperse in a single layer like templates $Cu_{2-x}S$ NCs #2 and #3 do, and some of #4 appear to. Coupled with the absorption spectra, it is possible that the variability in the NCs originates post synthesis. In samples #2-5, the NC size dispersion is relatively small, but the self-organization varies. This self-organization is largely affected by surface chemistry, so it is likely washing methods that then affect the final behaviour of the NCs. Later, this washing contribution is investigated.

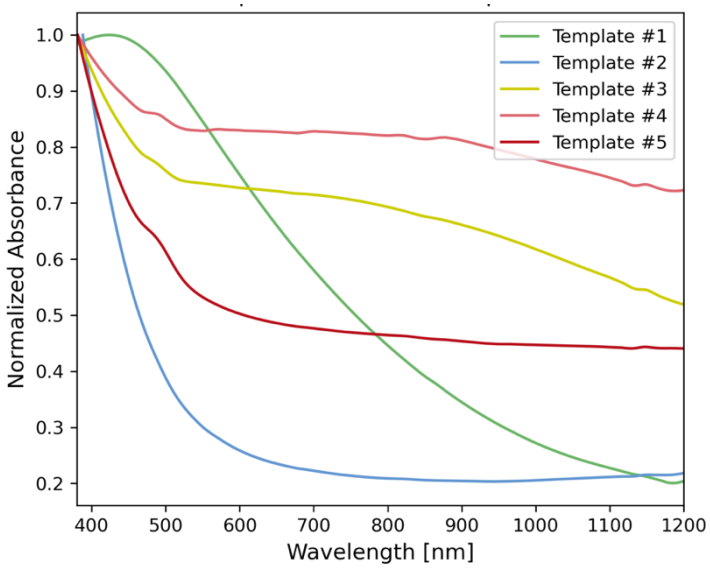

***Figure 3.1**: Normalized absorption spectra of templates $Cu_{2-x}S$ nanocrystals #1-5 synthesized by a seemingly identical procedure. Each sample is measured at what is assumed to be the same concentration, by assuming that all the copper from the precursor is consumed in the reaction. Spectra normalized in order to better compare the behaviour of all template nanocrystals in solution.*

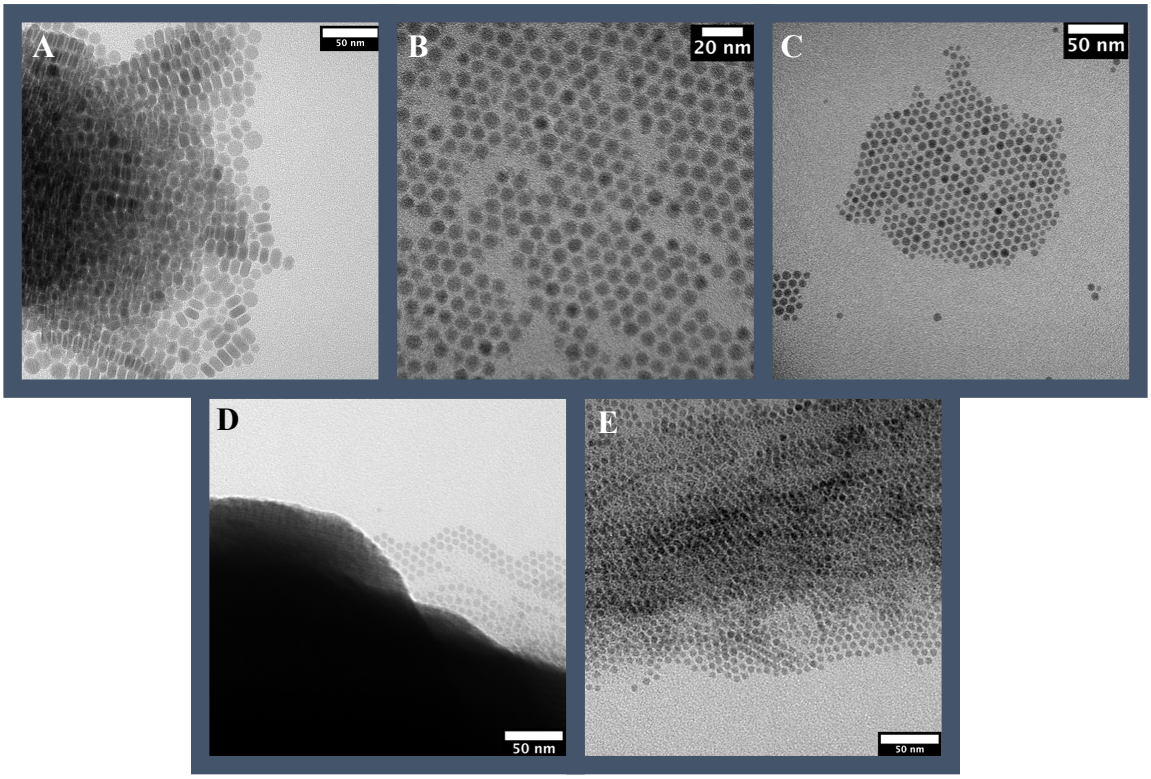

***Figure 3.2**: TEM images of each set of template $Cu_{2-x}S$ nanocrystals A. Templates #1, which appear to be platelets, with dimensions, length 14.9 ± 1.0 nm, and width 7.8 ± 1.0 nm. B. Templates #2, with dimensions, 6.5 ± 0.6 nm. C. Templates #3, with dimensions 6.2 ± 1.0 nm. D. Templates #4, with dimensions, 5.9 ± 0.6 nm. E. Templates #5, with dimensions 5.3 ± 0.5 nm.*

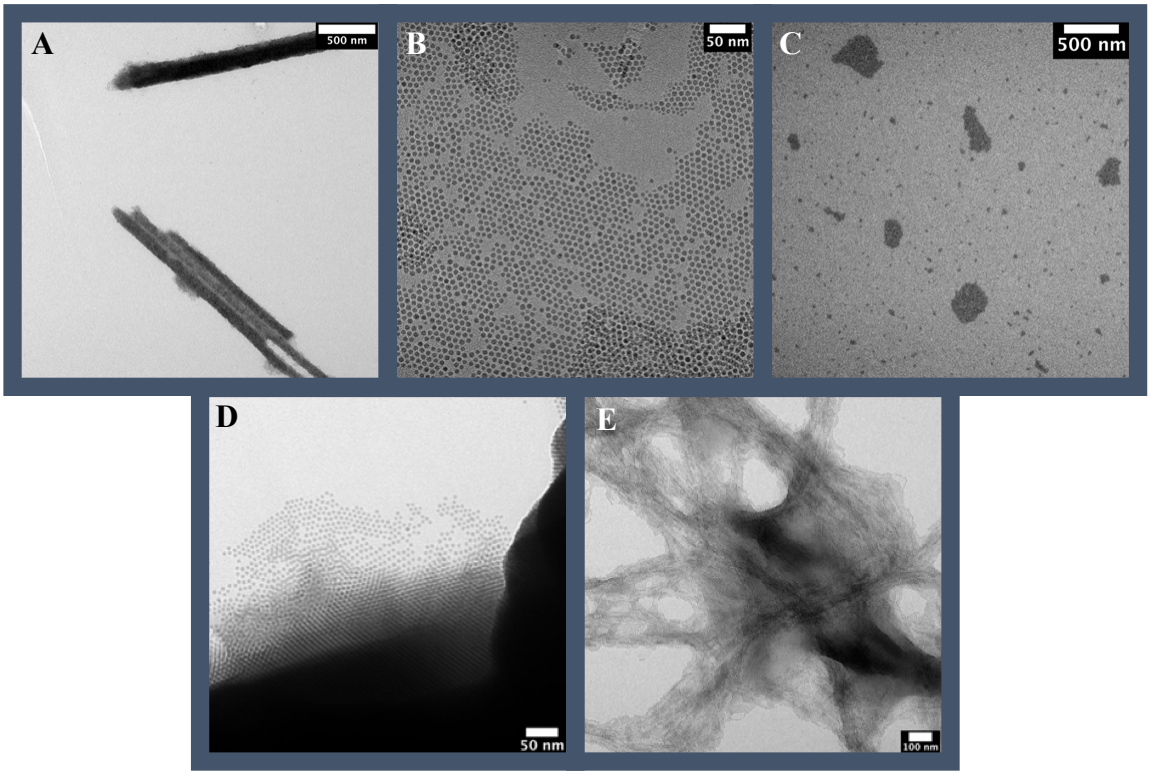

***Figure 3.3:** TEM images of each template $Cu_{2-x}S$ nanocrystals #1-5, in order listed A through E, as above in Figure 3.2. Lower magnification to show each sample. Aggregating behaviour and colloidal stability greatly varied between samples on the TEM grids and in solution.*

3.3.2 Indium precursor choice

Typically, in the procedures outlined by Xia et al,[1,2] the indium precursor is $In(OAc)_3$. However, this solid is not very soluble in ODE, especially when prepared outside of a Schlenk line, and as such, it was not a suitable choice for the scaled down reactions discussed in this thesis. It must be noted that the $In(OAc)_3$ experiments were tested out on the first templates which did not succeed, so no reaction was expected. Regardless of that, it was clear that it would be very difficult to achieve consistent concentration because the indium precursor was not homogeneous. Due to the low solubility of $In(OAc)_3$, it is difficult to determine whether the concentration of the precursor injected into each vial is constant with each cation exchange reaction. This tactic is impractical and therefore, this precursor was ruled out for further work. Absorption spectra of a selection from this set of experiments can be found below in Figure 3.4. Even with the addition of 2 times excess of precursor, there is no typical signature of cation exchange, as evidenced by the similarity of the absorption spectra of all of the different products to the templates $Cu_{2-x}S$ NCs #1 in Figure 3.1. Noting back to Figure 3.4, there is evidence of scattering, thus colloidal instability, and furthermore, the expected band-edge transition of $CuInS_2$ is not present, indicating no reaction.[2]

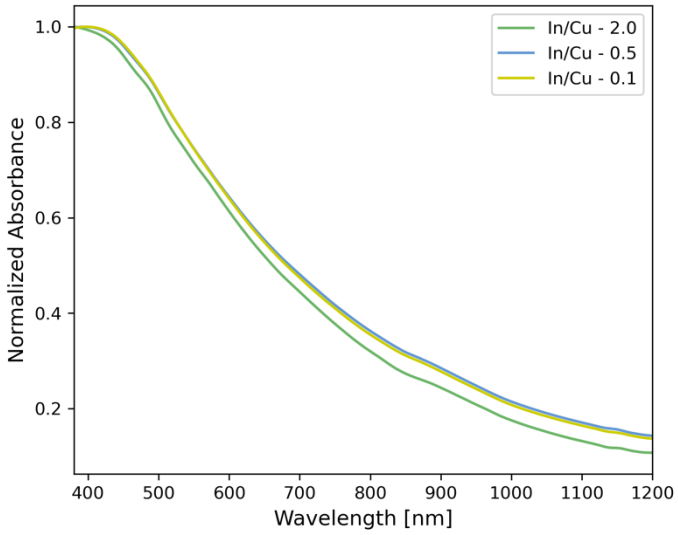

***Figure 3.4**: Normalized absorption spectra of a selection of reactions carried out with template $Cu_{2-x}S$ nanocrystals #1. Nanocrystals reacted with In/Cu = 2.0, 0.5 and 0.1.*

In the literature, indium chloride is also used as an indium source for this reaction.[9] This compound is soluble in ODE and therefore makes it a great candidate for the scaled down reactions in this work. Upon switching to using $InCl_3$ as the precursor, success was seen in a few cation exchange reactions (Figure 3.5), so this was chosen for further experiments. Here, success is defined as a cation exchange resulting in luminescent, stable NCs and is confirmed by the presence of the aforementioned expected band-edge transition. In Figure 3.5 below, in each set of cation exchanges, A-D, only the reactions with the greatest amount of indium precursor succeed, i.e., the reactions with In/Cu $\geq$1.0. The band-edge transition in these experiments is clearly visible. For lower precursor amounts, the absorption spectra are overpowered by scattering, meaning the colloidal particles are colloidally unstable. This was also evidenced by the cloudiness of the solutions, and the sedimentation of aggregates.

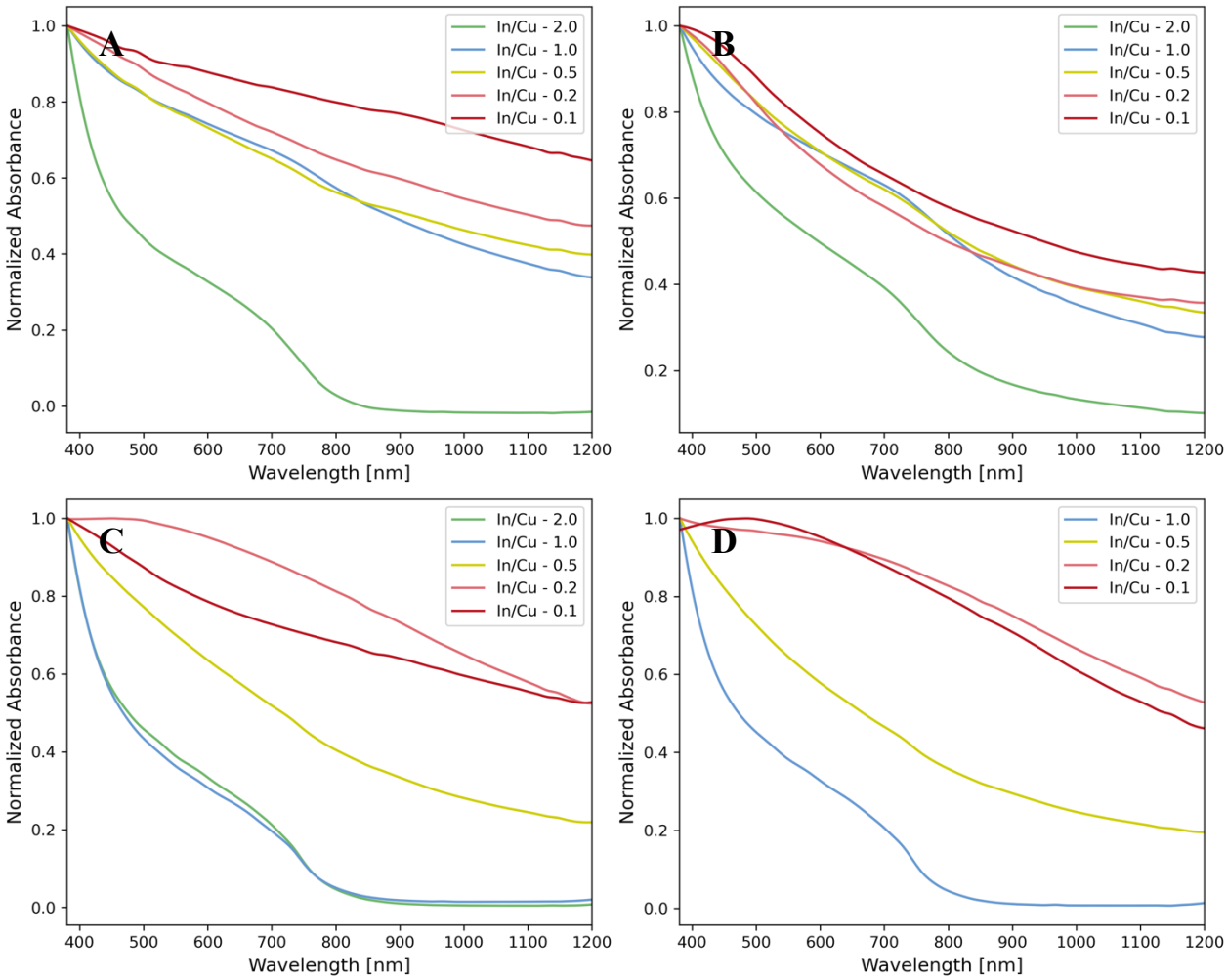

***Figure 3.5**: **A.** Normalized absorption spectra of cation exchange experiments with template $Cu_{2-x}S$ nanocrystals #2. **B.** Normalized absorption spectra of cation exchange experiments with template $Cu_{2-x}S$ nanocrystals #3. **C.** Normalized absorption spectra of cation exchange experiments with template $Cu_{2-x}S$ nanocrystals #4. **D.** Normalized absorption spectra of cation exchange experiments with template $Cu_{2-x}S$ nanocrystals #5.*

An aliquot of template $Cu_{2-x}S$ NCs in ODE was reacted for 1 hour at 125 ºC to investigate the effect of heating on the stability of the particles. As displayed in Figure 3.6, after heating with no precursor, the absorption spectra change significantly, and clearly shows signatures of light scattering. This indicated that the heating causes the NCs to aggregate. The absorption spectra of the cation exchange reactions at low precursor concentrations (Figure 3.5.A-D) matches with the one of the heated template $Cu_{2-x}S$ NCs, confirming that they become colloidally unstable.

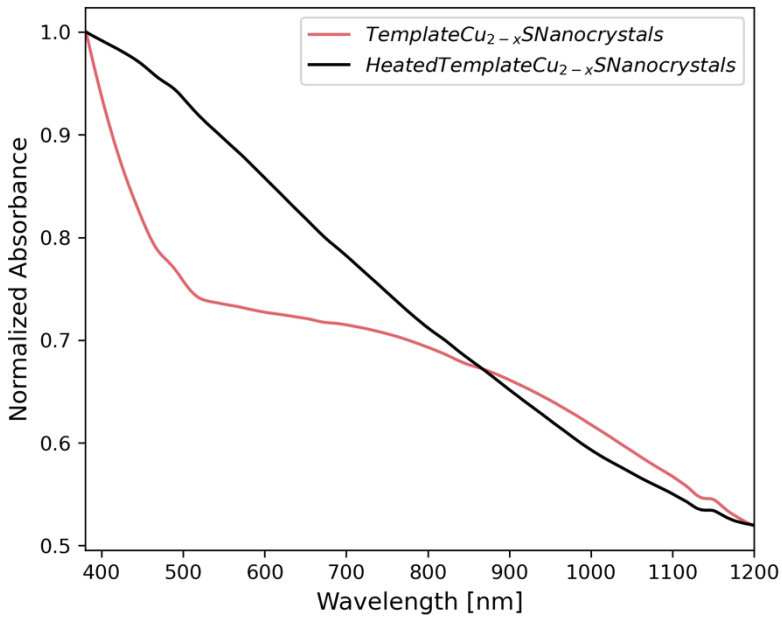

Figure 3.6: *Absorption spectra of original templates $Cu_{2-x}S$ nanocrystals #3, as compared to these nanocrystals after heating for 1 hour in ODE.*

3.3.3 Washing of $Cu_{2-x}S$ templates

To investigate the impact of the washing on the template $Cu_{2-x}S$ NCs, two new batches, #6 and #7, were prepared and an experiment was designed to see how the washing step of the templates could be used to bring all templates to the same starting point before cation exchange with an indium precursor.

The four washing methods trialed were,

I: 1 equivalent of antisolvent MeOH/BuOH

II: 2 equivalents of antisolvent MeOH/BuOH

III: 2 equivalents of antisolvent MeOH/BuOH & 50 µL toluene

IV: 2 equivalents of antisolvent MeOH/BuOH & 50 µL hexylamine

In Figure 3.7, it can be seen that in template $Cu_{2-x}S$ NCs #6, the first 3 washings result in very similar absorption spectra, and only washing method IV results in a differing spectrum. However, this curve is similar to those all of the washings of template $Cu_{2-x}S$ #7. This similarity can be seen in Figure 3.7 below, a peak is seen around ~ 350 nm, in sample template $Cu_{2-x}S$ #6 IV and all template $Cu_{2-x}S$ #7 washing samples.

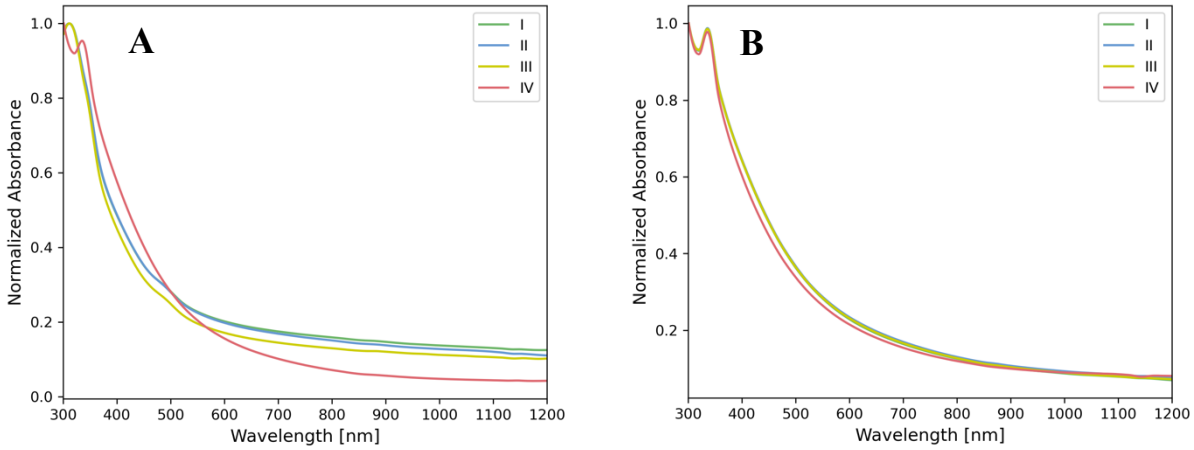

Figure 3.7: *Absorption spectra of templates $Cu_{2-x}S$ nanocrystals* ***A.*** *#6, and* ***B.*** *#7, after 4 different washings.*

Next, to see how this washing would affect the cation exchange, template NCs obtained using each washing method were subjected to a cation exchange reaction, with two In/Cu ratios, 1.0 and 0.5. In Figure 3.8, emission spectra of cation exchange reactions of both templates subjected to each washing method with two different In/Cu ratios is seen. When reacted with In/Cu =1.0, and template NCs #6, the sample with the most efficient PL is the sample washed by method IV, as evidenced by the most intense emission. When reacted with In/Cu =0.5, and template NCs #6, the sample with the most intense emission, is the sample washed by method II. When reacted with In/Cu =1.0, and template NCs #7, the sample with the most intense emission, is the sample washed by method IV. When reacted with In/Cu =0.5, and template NCs #7, the sample with the most intense emission, is the sample washed by method II.

Overall, the template NCs washed by method IV and reacted with In/Cu=1.0 resulted in the most luminescent NCs. The reason for this is unclear, but at least one factor contributing to this luminescence, is the fact that it is reacted with the greatest amount of precursor. The emission spectrum for this sample has the most intense PL. However, due to this promising result, all further cation exchanges in section 3.3.4 were carried out on template $Cu_{2-x}S$ NCs #6 that were treated with washing method IV. In the unnormalized spectra, this increased intensity is clear, and in the normalized spectra this can be seen by the improved signal/noise ratio in this sample. Normalized spectra are provided in Figure 3.8 to show that the peak position is constant despite the amount of $InCl_3$ precursor used. The dips in emission in these and all following spectra are attributed to solvent overtones, namely toluene in this case.

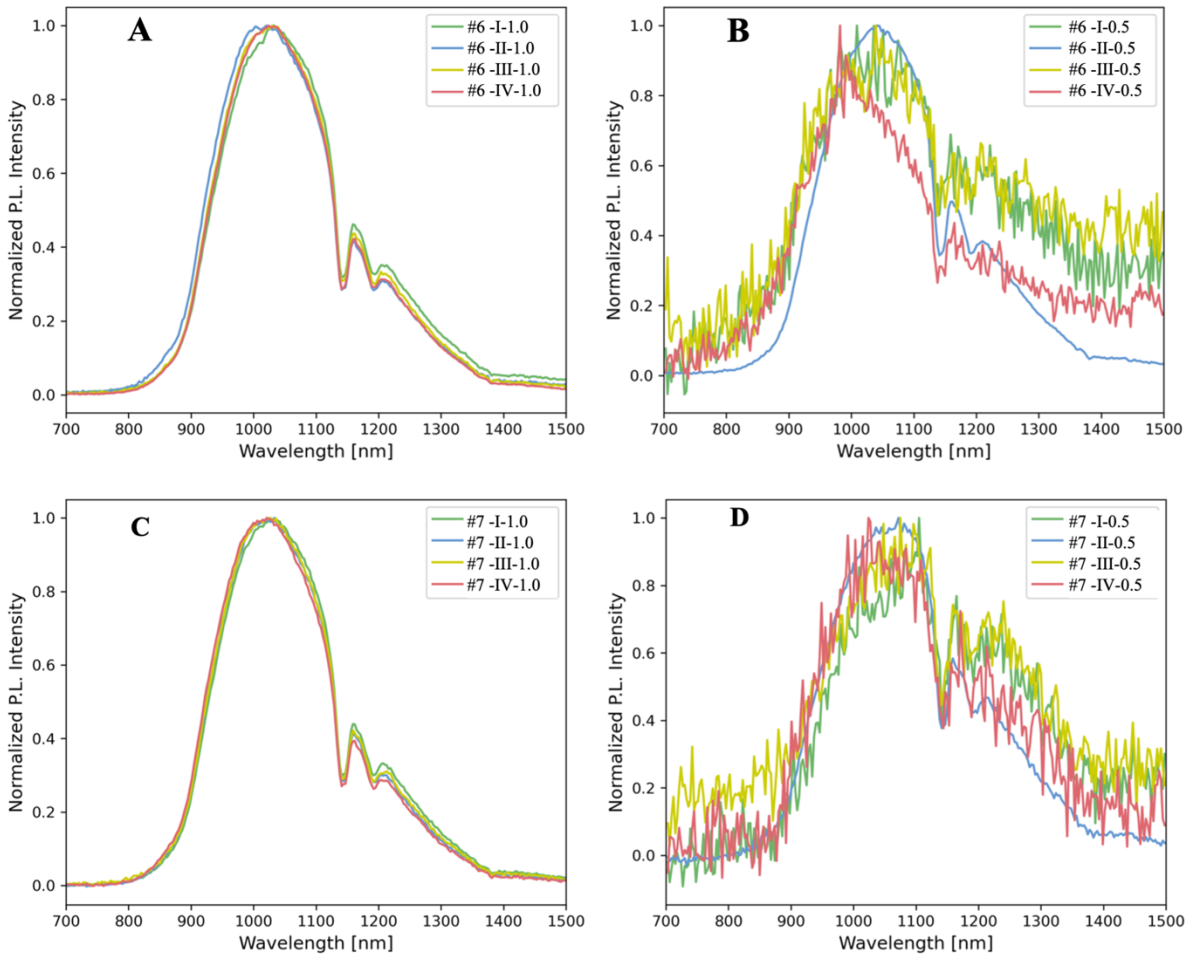

Figure 3.8: *Normalized emission spectra of* ***A.*** *Template $Cu_{2-x}S$ nanocrystals #6, subjected to each of the four washing methods, and then cation exchanged with In/Cu = 1.0.* ***B.*** *Template $Cu_{2-x}S$ nanocrystals #6, subjected to each of the four washing methods, and then cation exchanged with In/Cu = 0.5.* ***C.*** *Template $Cu_{2-x}S$ nanocrystals #7, subjected to each of the four washing methods, and then cation exchanged with In/Cu = 1.0.* ***D.*** *Template $Cu_{2-x}S$ nanocrystals #7, subjected to each of the four washing methods, and then cation exchanged with In/Cu = 0.5.*

3.3.3 Trioctlyphosphine Addition

As discussed before, cation exchange reactions using $InCl_3$ as a precursor were successful when In/Cu = 2.0 and 1.0 was used. Not only were those samples the most luminescent, but they were also the only colloidally stable samples after cation exchange.

To investigate why this may be the case, excess TOP was added to the reaction in two different ways to see if this would result in successful syntheses. This choice to investigate the effect of TOP was made because the In/TOP = 1 in the precursor solution, so, as the amount of In added to the reaction increases, so does the amount of TOP. Additionally, TOP plays two roles in this reaction, to act as a surfactant ligand and passivate the surface and to extract the Cu^+.[7,9,10]

Excess TOP addition was carried out in 2 ways. Firstly, TOP was added to the precursor solution as it was heating, and secondly, excess TOP was added directly to the templates $Cu_{2-x}S$ NCs #4, for a fixed amount of time, 3 minutes, prior to injection of the templates into the precursor solution. The fixed time was an arbitrary number chosen because it was believed to sufficiently expose the NCs to TOP without completely etching away the bulk of the templates which is known to be the case with these templates and TOP as

investigated by Nelson et al.[10] The amount of TOP was chosen to be 50μL, because in the reactions that succeeded previously, there was at least 50 μL of TOP in the indium precursor to begin with.

The TOP addition to both the precursors and the templates significantly changed the absorption spectra of the resulting $CuInS_2$ NCs (Figure 3.9). In Figure 3.9.A, C and E, the absorbance spectra shows that the characteristic band-edge transition at ~730 nm appears in both cases which was not evident before the addition of this excess TOP, due to the large contribution of light scattering to the measured spectra. Based on this data, and the samples in the cuvettes also becoming clear, it can be concluded that the addition of extra TOP provides colloidal stabilization of the NCs.

Given that TOP may etch $Cu_{2-x}S$ nanocrystal templates the timing of the exposure would have to be identical before every synthesis, so this method is likely less reproducible. Due to this, and the fact that the absorption spectra of the $CuInS_2$ NCs look similar whether TOP was added to the template or the precursor, for the next experiments, it was decided that the addition of excess TOP would be to the precursor solution. The TOP addition to cation exchanges using Templates #4 improves the emission of the NCs (Figure 3.9.B, D and F) but due to the colloidal instability of the templates NCs themselves, this increase is not consistent, and the signal/noise ratio remains quite low in all measurements. Despite this poor PL intensity, the peak position remains constant.

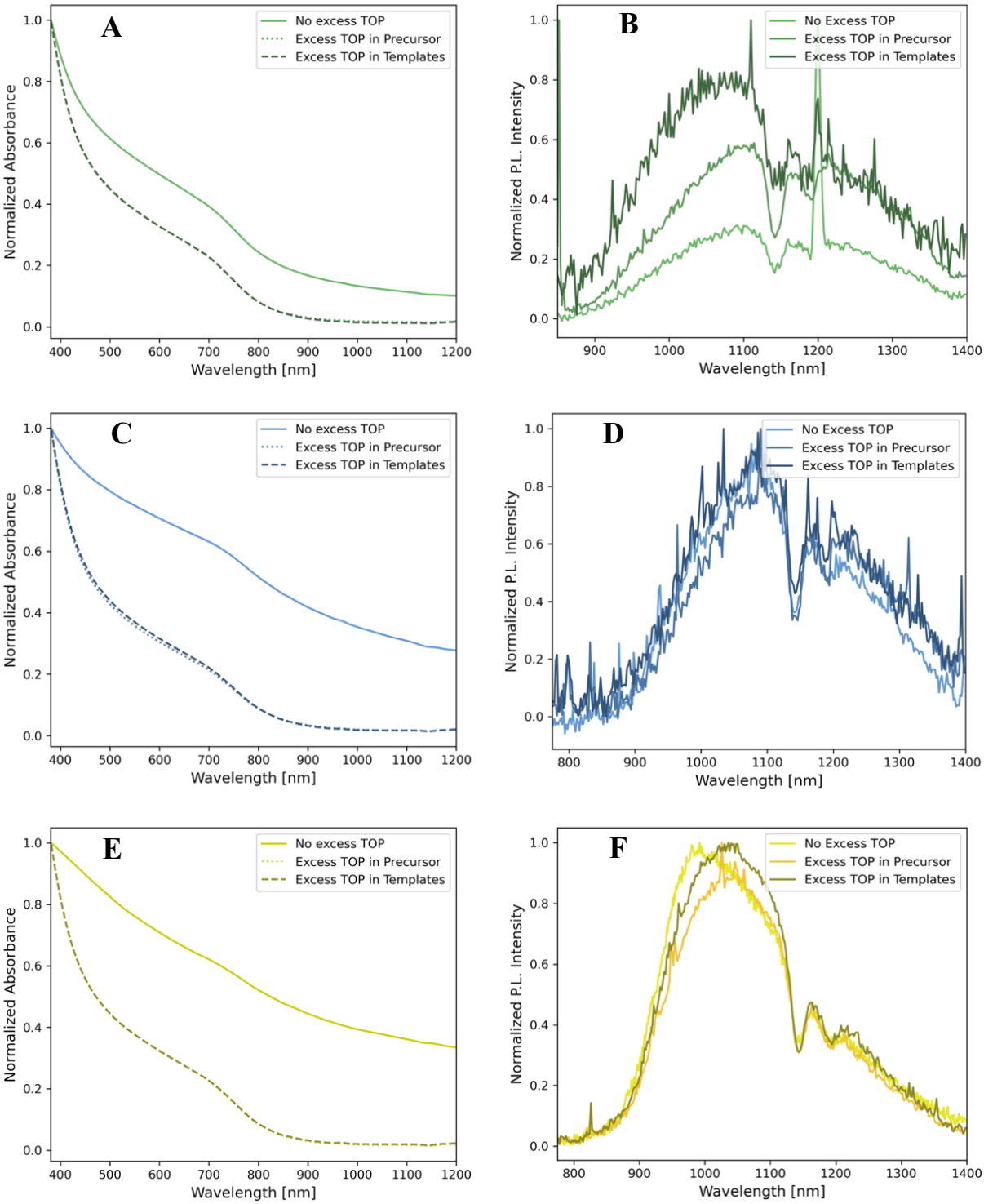

Figure 3.9: *Absorption and emission spectra of sets of reactions carried out with template $Cu_{2-x}S$ nanocrystals #4. Sets includes a control, with no excess TOP, and 2 reactions with 50 µL excess TOP each, one in the precursor and one directly in the nanocrystals. Nanocrystals exposed to excess TOP for 3 minutes.* ***A.*** *Absorption spectra and* ***B.*** *Emission spectra of set of reactions carried out with In/Cu = 2.0.* ***C.*** *Absorption spectra and* ***D.*** *Emission spectra of set of reactions carried out with In/Cu = 1.0.* ***E.*** *Absorption spectra and* ***F.*** *Emission spectra of set of reactions carried out with In/Cu = 0.5. (In Appendix A, Figure A1.2, these un-normalized absorbance spectra are shown)*

3.3.4 Tuning trioctlyphosphine addition

Considering the results from the washing experiments on templates $Cu_{2-x}S$ NCs #6 and #7, and the addition of TOP to templates $Cu_{2-x}S$ NCs #4, a more specific experiment combining these methods was designed to see which conditions would result in the most luminescent $CuInS_2$ NCs.

Template $Cu_{2-x}S$ NCs #6 were used as the base, with washing method IV as defined in the previous section. The control experiment was carried out as experiments before, with each sample containing the same amount of template, and decreasing amounts of the stoichiometric $InCl_3$-TOP precursor. For these experiments, five different In/Cu ratios were investigated, and for each there was a control, with no excess TOP, an addition of 16 µmol of TOP and also 47 µmol of TOP in the precursor. The five ratios of In/Cu were 1, 0.5, 0.25, 0.2 and 0.15.

In Figure 3.10, the total TOP/In ratios that relate to these In/Cu ratios are all 1:1, in the no excess TOP case. Figure 3.10.A, the experiments show that only the samples with the greatest amount of indium precursor (In/Cu = 1.0) clearly shows the band-edge transition at 720. This result is consistent with previous experiments. This solution contains the greatest amount of TOP in this set of cation exchange experiments. The rest of the samples are completely destabilized as is the case in In/Cu = 0.15, as compared to the heating template test mentioned in Figure 3.6. This is also reflected in the emission of this set of reactions, Figure 3.12.B, where only the sample In/Cu = 1.0 results in a detectable emission spectrum, as compared to the rest of the samples which show no significant emission at the expected peak range 1050 – 1250 nm.[6]

As shown in Figure 3.10.C, upon the addition of 16 µmol of TOP to each sample, in each case, the band-edge transition begins to be evident. It is seen at 720 nm for samples In/Cu = 1.0 through 0.25, at 712 nm for In/Cu = 0.2 and at 717 nm for In/Cu = 0.15. In the samples with In/Cu = 0.25, 0.2, 0.15, there is still a significant amount of scattering. These positions of the band-edge transition are calculated using the minimum of the second derivative of the absorption spectrum, (see Figure A1.4.B). Upon examination of the emission of these samples, Figure 3.10.D, once again the sample with In/Cu = 1.0, shows the highest intensity as evidenced by the high signal/noise ratio. The peak position is the same in all cases, despite the low signal/noise ratio of most spectra.

Lastly, in the case of adding 47µmol of TOP, in Figure 3.10.E, these spectra of all the different samples look quite similar, with the band-edge transition appearing clearly in each sample, at 712 nm for In/Cu = 1.0 through 0.25 and 725 nm for In/Cu = 0.2 (Appendix A, Figure A1.4.C). The transition is clear even those with previously significant scattering that was overshadowing this feature. In the emission spectra, Figure 3.10.F, the emission intensity is significantly higher in all samples, allowing the acquisition of spectra with high signal/noise ratio. All peaks appear in the expected range.

In conclusion, there is a clear increase in emission intensity as the amount of excess TOP is increased, and the expected increase with increasing amounts of indium precursor (containing increasing amounts of TOP), as the photoluminescent response of the NCs increases as they become more indium rich.[11] There is also seemingly a limit to the emission of some samples such as In/Cu = 1.0. (Figure A1.3, unnormalized spectra show no increase in PL signal from 16 to 47 µL of excess TOP.)

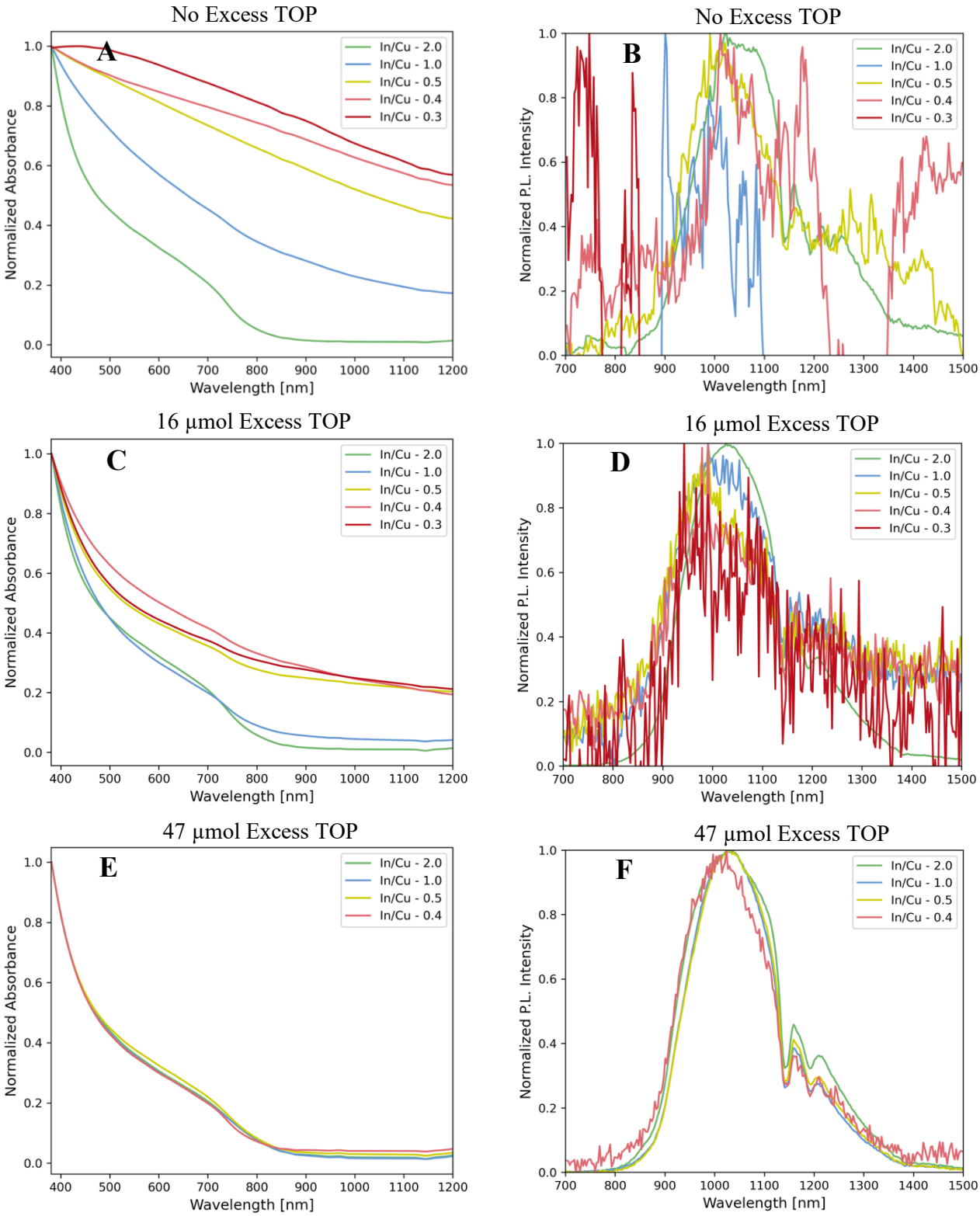

***Figure 3.10**: Normalized absorption and emission spectra of three sets of cation exchanges carried out with template $Cu_{2-x}S$ NCs #6, using washing method IV, as previously defined. **A.** Absorption spectra and **B.** Emission spectra of control set of experiments, cation exchange with no excess TOP addition. TOP/In ratio 1:1 in all cases. **C.** Absorption spectra and **D.** Emission spectra of set of experiments with 16 µmol excess TOP added to the $InCl_3$ precursor. TOP/In ratios of 1.36, 1.73, 2.45, 2.78 and 3.29 corresponding respectively to the In/Cu ratios of 1.0, 0.5, 0.25, 0.2, 0.15. **E.** Absorption spectra and **F.** Emission spectra of set of experiments with 47 µmol excess TOP added to the $InCl_3$ precursor. TOP/In ratios are as follows, 2.06, 3.14, 5.27, 6.22, corresponding respectively to the In/Cu ratios of 1.0, 0.5, 0.25, 0.2. Unnormalized emission spectra can be found in Appendix A, Figure A1.3.*

To verify whether the addition of TOP was not etching the NCs, the size of the NCs was investigated prior to and after the TOP addition. Figure 3.11 A and B shows that the addition of excess TOP does not significantly alter the size of the exchanged NCs as compared to the template NCs. This indicates that TOP does not etch the NCs in a significant manner if at all. In Figure 3.12, STEM images of the templates NCs #6 in A, and cation exchanged NCs, B, are shown to demonstrate the narrow size dispersion of the sample and shape preservation of the NCs.

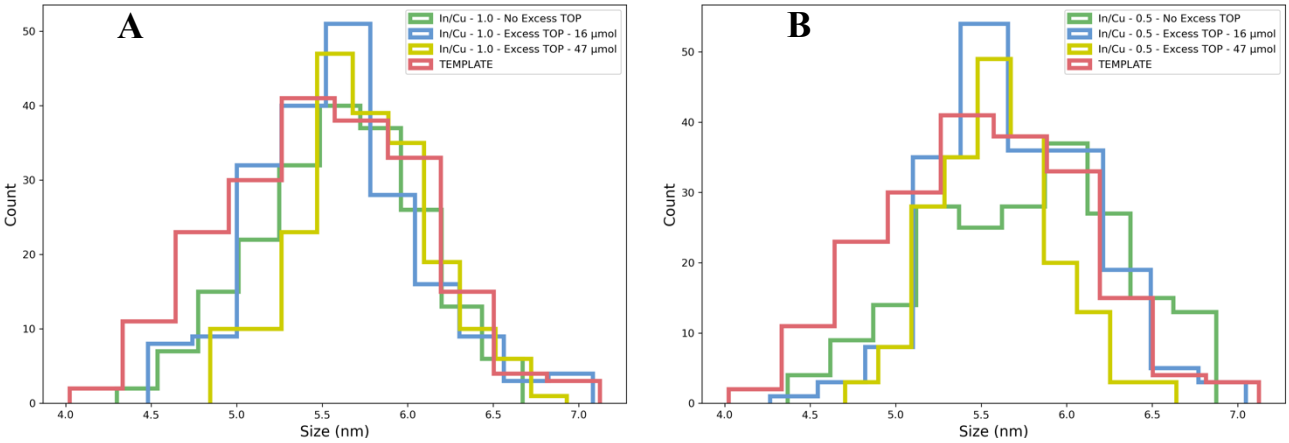

Figure 3.11: *Histograms representing the size measurements of cation exchanged samples.* ***A.*** *Size measurements of template $Cu_{2-x}S$ nanocrystals #6, washed by method IV, cation exchanged with In/Cu = 1.0. Control, 16 µmol excess TOP, and 47 µmol excess TOP, compared to bare copper sulfide template nanocrystals #6 washed by method IV.* ***B.*** *Size measurements of template $Cu_{2-x}S$ nanocrystals #6, washed by method D, cation exchanged with In/Cu =0.5. Control, 16 µmol excess TOP, and 47 µmol excess TOP, compared to bare copper sulfide template nanocrystals #6 washed by method IV.*

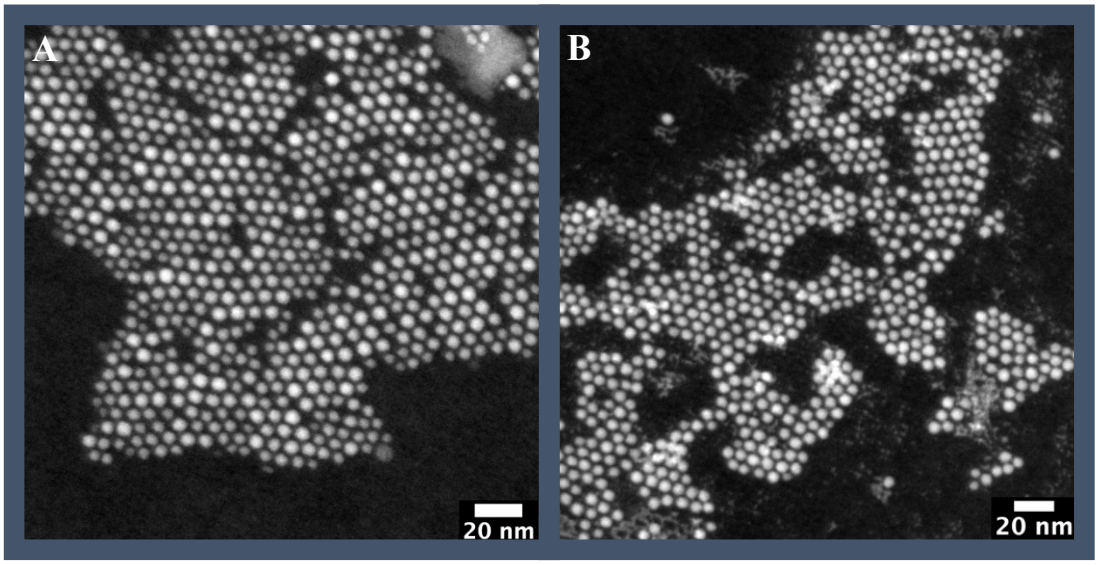

Figure 3.12*: **A**. STEM image of $Cu_{2-x}S$ nanocrystals, templates #6. 5.52 ± 0.56 nm.* ***B.*** *STEM image of template #6 $CuInS_2$ nanocrystals cation exchanged with In/Cu = 1.0, and 47 µmol excess TOP added in the $InCl_3$ precursor. 5.76 ± 0.39 nm.*

Elemental analysis shows that despite the amount of excess TOP added there is a limit to how much indium may be incorporated into the NCs, (Figure 3.15). TOP is a soft Lewis base and thus has an affinity for soft Lewis acids, such as Cu^+. A mentioned previously, one of the roles of the TOP in this reaction is to couple with and extract the Cu^+ ions in order to create vacancies for the incorporation of In^{3+} in the framework.[7,9] This is possible when it to bound to $InCl_3$ as a complex[7,9] and when it is free in solution.[10] In this mechanism, TOP affects the reaction rate, and has kinetic control of the cation exchange. The more TOP that is available, the more Cu^+ it can extract and thus the more In^{3+} can be incorporated. Additionally, to ensure a charge balance, 3 Cu^+ must be removed in order for one In^{3+} to be incorporated into the framework. Thus, the reactions with a lower overall amount of TOP (those with the lowest In/Cu), have less or slower incorporation of In^{3+}. It is then possible that the sets of reactions with less TOP perhaps do not go to completion in the given 1 hour of reaction, resulting in sub-stoichiometric $CuInS_2$ NCs. In the case of In/Cu = 1.0, there is quite a high ratio beyond 1.0, we attribute it to the limitations of the washing steps of these particles as some precursor indium could be left behind. Also, the counts for some of the measurements were quite low resulting in large margins of error in some cases.

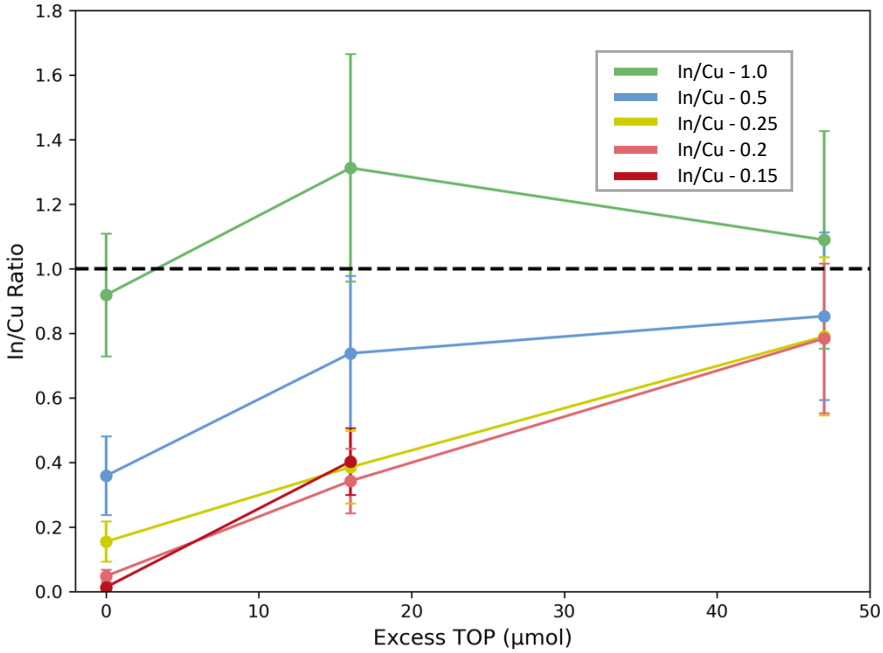

***Figure 3.13**: Graph showing the In/Cu ratio from elemental analysis post cation exchange in each set of reactions, control, 16 µmol excess TOP and 47 µmol excess TOP.*

3.3.5 Gallium incorporation into $CuInS_2$ nanocrystals

To investigate the feasibility of gallium incorporation into the wurtzite $CuInS_2$ NCs, some preliminary tests were carried out according to the procedure laid out by Hinterding et al.[7] for chalcopyrite NCs. This was done by preparing four different Ga^{3+} precursor solutions, in different solvents, toluene or ODE, with ligands DDT or DPP. These experiments were carried out on wurtzite $CuInS_2$ NCs provided by Raimon Terricabres-Polo, synthesized using the stoichiometric In/TOP precursor, with no excess TOP. Figure 3.14 features the absorbance and emission spectra of the $CuInS_2$ NCs subjected to reaction with the Ga^{3+} precursor. Both ligands result in increased luminescence and a blue shift of approximately 50 and 100 nm using

DDT and DPP respectively. The greater blue shift is observed when DPP is used as the ligand. Additionally, the higher signal/noise ratio of the Ga^{3+}/DPP sample, indicated that this method increases the luminescence of the NCs to a greater extent than Ga^{3+}/DDT. The reaction does not proceed when ODE is used as the solvent for the cation exchange, the template NCs become colloidally unstable, and as such these samples were not measured. When considering the previous cation exchange reactions and this set, the templates are kept in a solution of 50/50 ODE/DDT, whereas here, the template $CuInS_2$ NCs are originally in toluene. This suggests that only a reaction between a precursor and template in the same solvent would proceed. Figure 3.15 shows a TEM image of $CuInS_2$ NCs reacted with Ga^{3+}, with DDT as the ligand. The elemental composition of these exchanged NCs is Ga: 33.4 %, Cu: 14.6 %, In: 9.35 %, S: 42.6 %. These elemental fractions were measured after 1 washing step, so it is possible that there is still left-over gallium from the precursor. However, in tandem with the absorption and emission spectra, this observation provides strong evidence that gallium has indeed been incorporated into the $CuInS_2$ template NCs. Based on these results, it can be concluded that the treatment of wurtzite $CuInS_2$ NCs by Ga^{3+} cation exchange protocols that work for chalcopyrite $CuInS_2$ NCs is effective using either DPP or DDT as ligands, and toluene as a solvent.

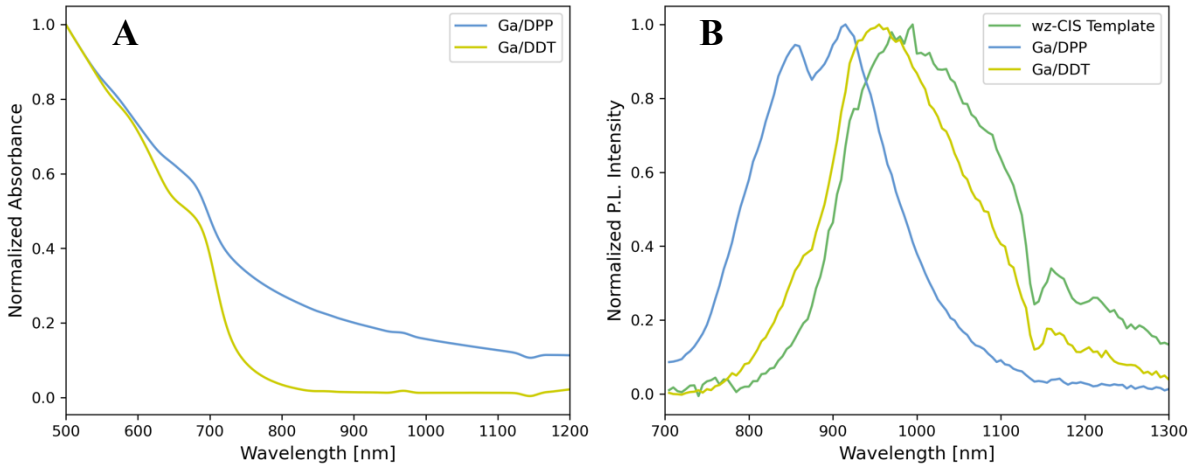

Figure 3.14: A. *Absorption spectra of nanocrystals after Ga^{3+} incorporation.* ***B.*** *Emission spectra of nanocrystals after Ga^{3+} incorporation. Dips in emission around 850 and 1150 nm are due to toluene solvent overtones.*

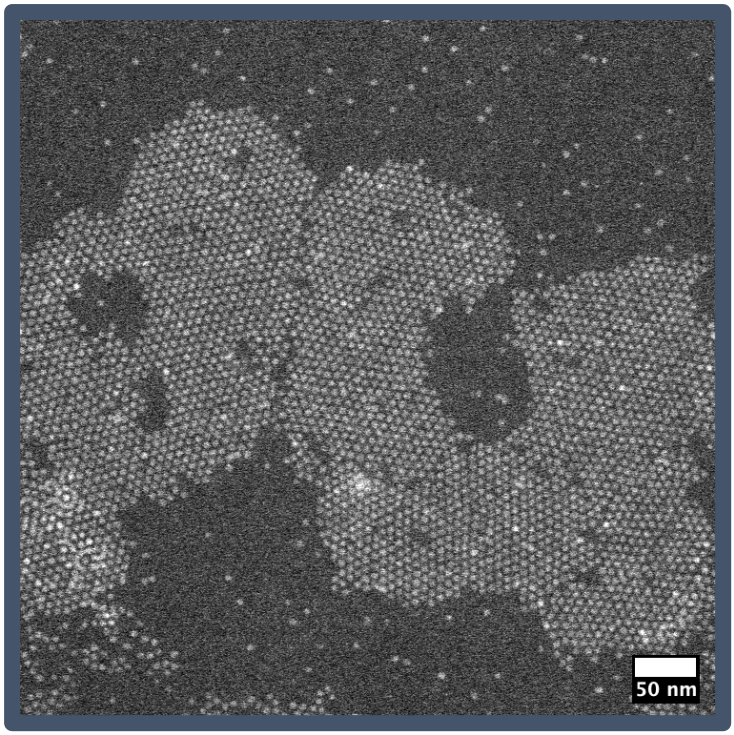

Figure 3.15: *TEM image of $CuInS_2$ template nanocrystals after cation reaction with Ga^{3+}/DDT precursor.*

3.4 Conclusion and Outlook

The published procedures for the synthesis of $Cu_{2-x}S$ NC templates were not consistently reproducible. Additionally, the cation exchange procedures outlined were only successful with a high In/Cu ratio. By carrying out many investigative cation exchange reactions, we determined that it was possible to wash $Cu_{2-x}S$ template NCs synthesized at different times in order to bring them to a similar starting point before the process of cation exchange begins. Next, we conclude that it is possible to synthesize luminescent $CuInS_2$ NCs even with low amounts of indium precursor, by the addition of excess TOP to the precursor, which stabilizes the NCs. Lastly, we show that it is possible to improve the luminescence of these wurtzite $CuInS_2$ NCs upon cation exchange with Ga^{3+}/DPP or DDT complex. This improvement has been shown by Hinterding et al,[7] on chalcopyrite $CuInS_2$ and our work concludes that the same procedures are effective for the wurtzite. This exchange results in a blue shift and increased luminescence.

For future experimentation, such that these NCs could become good candidates for LSC use, more cation exchange experiments should be designed to test the influence of extended time on the cation exchange. Additionally, the Ga^{3+} experiments should be tested with the most luminescent particles that resulted from the excess TOP trials to see if this incorporation could surpass the apparent limit of luminescence.

3.5 References

[1] Xia, C., Meeldijk, J. D., Gerritsen, H. C., & de Mello Donega, C. Highly Luminescent Water-Dispersible NIR-Emitting Wurtzite $CuInS_2$/ZnS Core/Shell Colloidal Quantum Dots. *Chem. Mater*. *29*(11), 4940–4951, (2017).

[2] Xia, C., et al. Size-Dependent Band-Gap and Molar Absorption Coefficients of Colloidal $CuInS_2$ Quantum Dots. *ACS Nano.* 12, 8350-8361, (2018).

[3] Li L, Pandey A, Werder D, et al. Efficient synthesis of highly luminescent copper indium sulfide-based core/shell nanocrystals with surprisingly long-lived emission. *J. Am. Chem, Soc.* 133(5), 1176-1179, (2011).

[4] Tomic, S., Bernasconi, L., Searle, B.G., Harrison, N.M. Electronic and Optical Structure of Wurtzite $CuInS_2$. *J. Phys. Chem. C.* 118, 26, 14478–14484, (2014).

[5] Ning J, Kershaw S, Rogach A. Synthesis and Optical Properties of Cubic Chalcopyrite/Hexagonal Wurtzite Core/Shell Copper Indium Sulfide Nanocrystals. *J. Am. Chem, Soc.* 44, 141, (2019).

[6] Liu, X., et al. Size-Controlled Synthesis of $Cu_{2-x}E$ (E = S, Se) Nanocrystals with Strong Tunable Near-Infrared Localized Surface Plasmon Resonance and High Conductivity in Thin Films. *Adv. Funct. Mater.* 23, 1256–1264, (2013).

[7] Hinterding, S.O.M., et al. Tailoring Cu^+ for Ga^{3+} Cation Exchange in $Cu_{2-x}S$ and $CuInS_2$ Nanocrystals by Controlling the Ga Precursor Chemistry. *ACS Nano.* 13, 12880-12893, (2019).

[8] Li, C., et al. A Simple Method to Clean Ligand Contamination on TEM Grids. *Ultramicroscopy.* 221, 113195, (2021).

[9] van der Stam, W., et al. Near-Infrared Emitting $CuInSe_2$/$CuInS_2$ Dot Core/Rod Shell Heteronanorods by Sequential Cation Exchange. *ACS Nano*. 9(11), 11430-11438, (2015).

[10] Nelson, A., Ha, D., Robinson, R.D. Selective Etching of Copper Sulfide Nanoparticles and Heterostructures through Sulfur Abstraction: Phase Transformations and Optical Properties. *Chem. Mater*. 28, 8530−8541, (2016).

[11] Tapley, A., et al., Preparation and characterization of $CuInS_2$ nanocrystals for photovoltaic materials. *Phys. Chem. Chem. Phys.* 15, 1431-1436, (2013).

4. Tailoring Cd for In exchange in InSb nanowires

4.1 Introduction

As mentioned in the section 2.4.2, InSb nanowires are an attractive material for quantum computing, due to their high spin orbit coupling and high electron mobility.[1,2,3] In addition to this, there is a large amount of electron scattering at the surface of the nanowires. For use in quantum computing this electron scattering poses a problem so there is a need to modify the surface in a way that will limit this. InSb is a very covalent III-V semiconductor material and so it is not expected to change when subjected to post-synthetic modification reactions. Despite this, this work investigates the discovery of the total metal exchange of InSb to Cd_3Sb_2. CdSb is a material which also has a small bandgap, high electron mobility and it also has low thermal conductivity and Cd_3Sb_2 is the metastable form of this compound. This material cannot be synthesized from scratch, so this discovery is very beneficial.

The serendipitous discovery of the total metal exchange occurred upon the addition of excess $Cd(oleate)_2$ to the effort to grow CdTe shells. Upon the addition of excess material, the reaction completely forgoes the shell growth and instead results in a Cd^{2+} for In^{3+} cation exchange. The shell growth was expected to be successful due to the very small lattice mismatch of InSb and CdTe. Actually, the success of the shell growth experiment before happened due to arsenic contamination of the wires due to the starting material. New wires were grown without arsenide-based chemicals and thus this contamination was missing, so the shell growth was not reproducible. And because the surface free energy of InSb is low, and the material is expected to be extremely unreactive, the happenstance of the Cd for In metal exchange is very surprising. The following experiments are the result of tailoring this metal exchange to final optimal conditions for the exchange of all nanostructures in a sample.

The success of this reaction led to experimentation with other metal oleates to see how the reaction proceeds if at all in these scenarios and it was found to be unique to the $Cd(oleate)_2$ reaction.

4.2 Experimental

4.2.1 Chemicals

Toluene (Alfa Aesar, anhydrous, 99.8%), 1-Octadecene (ODE, Thermo Scientific, 90%, degassed), Oleic acid (OA, Sigma-Aldrich, 90%), Cadmium Oxide (CdO, Sigma-Aldrich, 99%)

4.2.2 Synthesis

Except where noted otherwise, all reactions and washing steps were carried out in a glovebox under nitrogen atmosphere, $[O_2] \leq 3$ ppm and $[H_2O] = 0$ ppm

4.2.2.a Nanowire Synthesis

The nanowires were synthesized by Ghada Bhadawy from the Department of Applied Physics, at the Eindhoven University of Technology. The wire growth is detailed in, High Mobility Stemless InSb Nanowires[1], for the interested reader.

4.2.2.b Cadmium oleate synthesis

In a Schlenk line, 80 mmol of OA and 20 mmol of CdO were combined in a 3-neck flask (a rusty red mixture). The mixture was degassed at 100 ºC for 30 minutes and then heated

to 190 ºC under nitrogen (turns clear/yellow). The mixture was kept at 190 ºC for 20 minutes and then cooled to 110 ºC and degassed for 20 minutes. Upon cooling to room temperature, 10 mL acetone was added to precipitate $Cd(oleate)_2$, (immediately turned a cloudy white), centrifuged at 1471 RCF (2750 RPM) for 10 minutes, then the supernatant was discarded. To ensure that all excess OA was removed, such that the addition of the excess can be controlled, the solid was washed four more times with the same procedure. The solid was dried over 48 hours under vacuum.[2] This solid was used to make 10^{-3} M $Cd(oleate)_2$ in ODE. Excess oleic acid was added directly to the $Cd(oleate)_2$ solution in ODE.

4.2.2.c Cd for In exchange

The exchange was carried out by placing an InSb nanowire wafer in a small vial containing 2 mL of 10^{-3} M $Cd(oleate)_2$ with $4x10^{-3}$ M excess OA on a hot plate at 50 ºC. (To investigate the role of OA, a series of experiments were carried out using different amounts of excess OA, 0 M, $2x10^{-3}$ M, $4x10^{-3}$ M, $6x10^{-3}$ M, and 10^{-2} M). This vial was sealed and heated to 180 ºC. Once the reaction vessel reached this temperature, the reaction time began. Reaction time was varied depending on desired amount of cation exchange. Upon completion of reaction, the vial was removed from the hot plate, allowed to cool to room temperature, and then the wafer was rinsed with 5 mL aliquots of toluene a minimum of five times to remove all excess precursor solution. After washing, the sample was allowed to dry. TEM grids were prepared by swiping copper grids along the wafers. The wafers were used as is for SEM imaging.

4.2.3 Characterization

Transmission electron microscopy (TEM) images were taken with a Thermo Scientific Talos F200X transmission electron microscope, with an accelerating voltage of 100 or 120 kV. Scanning transmission electron microspcopy (STEM), and high-angle annular dark-field imaging (HAADF) images were used to measure nanowire and wedge sizes. Nanostructures were measured by hand in the program FIJI. Energy dispersive X-ray spectroscopy (EDS) measurements were performed with the Talos TEM equipped with a Field Emission Gun, and 4 SDD Super-X detectors. TEM grid samples prepared by swiping the copper grid along the surface of an InSb wafer after reaction.

Scanning electron microscopy (SEM) images were taken with a Thermo Scientific desktop Phenom ProX scanning electron microscope. This instrument is fitted with an SDD Energy-dispersive X-ray detector for elemental mapping and analysis.

X-Ray Diffraction (XRD) analysis carried out with a Malvern PANalytical AERIS instrument using entire pristine and reacted InSb wafers.

4.3 Results and Discussion

The nanowires are grown on small InSb substrate wafers, and a byproduct of this nanowire growth synthesis are nanoflakes which have the same zinc blende crystal structure as the wires but with greater dimensions. These flakes are convenient for tracking the cation exchange in this experiment because they take longer to completely transform. In this discussion section, these flakes are used for analysis as well as the nanowires, but in general the ensemble is referred to as nanowires.

To paint a picture of the system we are working with, in Figure 4.1 below, one can see the nanostructures on the InSb wafers, A and B, showing wafers from different nanowire

batches. From the overview in Figure 4.1.A and C, one can see nanowire fields of different sizes, and in Figure 4.1C the varying nanowire density is also clear. Figure 4.1D through E, show various fields at the same magnification and the varying density and distribution of the nanowires. It is understood that these are samples after reaction, and washing, and additionally exposed to air to be measured by SEM. It is however clear that these fields must also be this diverse before reaction and can therefore affect the results of the exchange.

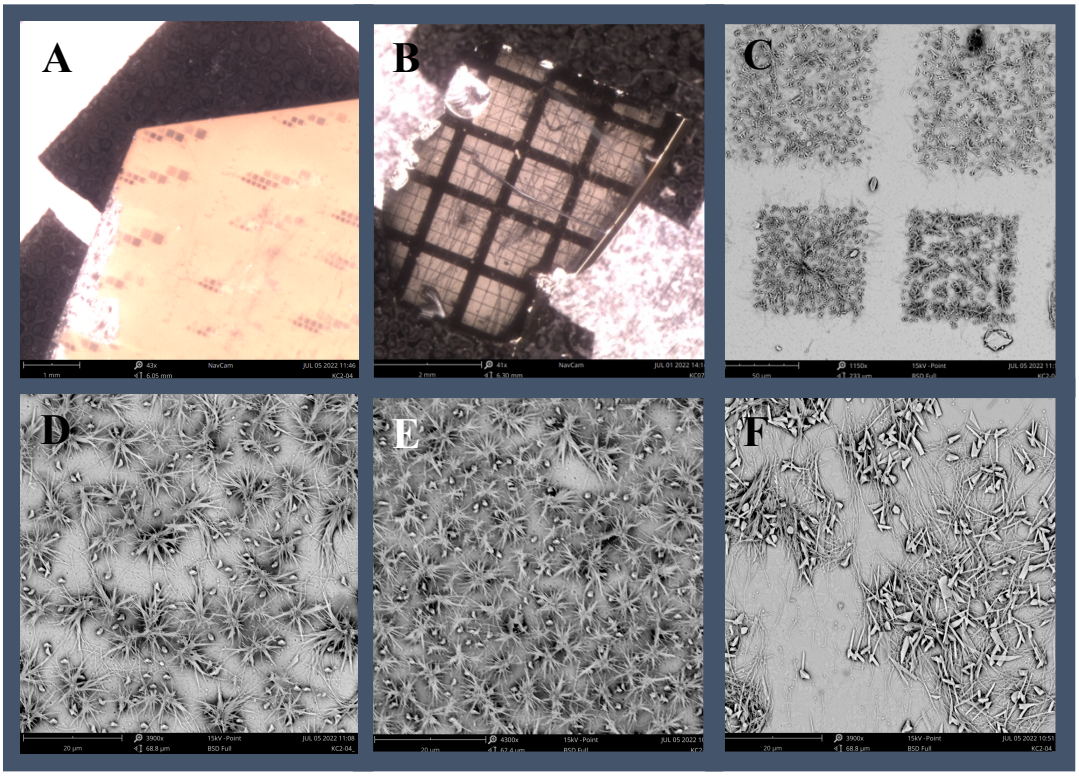

Figure 4.1: ***A.*** *SEM image of a wafer containing several fields of InSb nanowires from one batch of samples. Scale bar = 1 mm.* ***B.*** *SEMOverview of a wafer of InSb nanowires from a different batch of samples (all same diameter).* ***C.*** *Magnification of the wafer shown in A highlighting four different fields of nanowires. Scale bar = 50 µm..* ***D, E, F,*** *Higher magnification SEM images of a different nanowire fields from the wafer shown in A. Scale bars = 20 µm.*

4.3.1 Temperature

The reaction temperature of 180 ºC was chosen based on preliminary experiments carried out by Serena Busatto. As shown in Figure 4.2, reaction conditions for these experiments were 2 hours at 110 ºC, 150 ºC or 180 ºC. After 2 hours, In was completely replaced by Cd only at 180 ºC. This indicates that there is an activation energy of the reaction that must be overcome in order for the reaction to proceed.

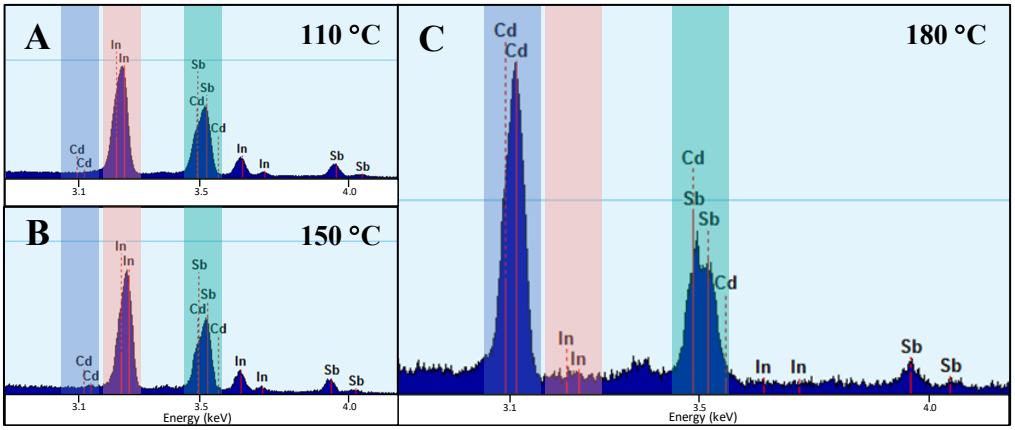

Figure 4.2: EDS spectra of the nanowires after reaction with Cd(oleate)$_2$ for 2 hours at A. 110 °C, B. 150 °C and C. 180 °C

4.3.2 Influence of reaction time

The reaction progress at 180 °C under 10^{-3} M Cd(oleate)$_2$, was tracked ex-situ by TEM (Figure 4.3). After 30 minutes, (Figure 4.3.A), there is partial transformation of some wires, while most of the nanowires remain completely pristine. The partial transformation is inferred from the observation of small triangular domains. After 60 minutes of reaction, (Figure 4.3.B), there is a greater number of nanowires with the triangular domains. There are still however, many wires with no evidence of changes at all. Finally, after ≥ 80 minutes, Figure 4.3C, there is complete transformation of the nanowires and the nanoflakes in the samples.

As depicted in Figure 4.4, elemental analysis by EDS shows that the triangular domains are cadmium rich. An area with one of these wedges was analyzed (Figure 4.4.A) and determined to have cadmium, indium and antimony present. The intensity of the In peak with respect to the Sb peak has decreased, this implies that the In was exchanged by Cd. To compare, an area with no triangular domains, Figure 4.4.B, was also examined by EDS and in this area, only indium and antimony are found, in a stoichiometric ratio, indicating that this is the pristine starting material.

Elemental mapping was also carried out on areas of the wires containing these triangular domains, (Figure 4.5), and they are shown to be Cd-rich areas which penetrate the depth of the nanowires. From this point forward, these areas will be referred to as wedges. Thus, we can conclude that the remaining presence of indium of reacted wires can be explained by the notion that the wedge does not penetrate all the way through the whole wire, and because this method analyses the composition through the whole diameter of the wire, of course there will still be starting material remaining underneath the exchanged domain.

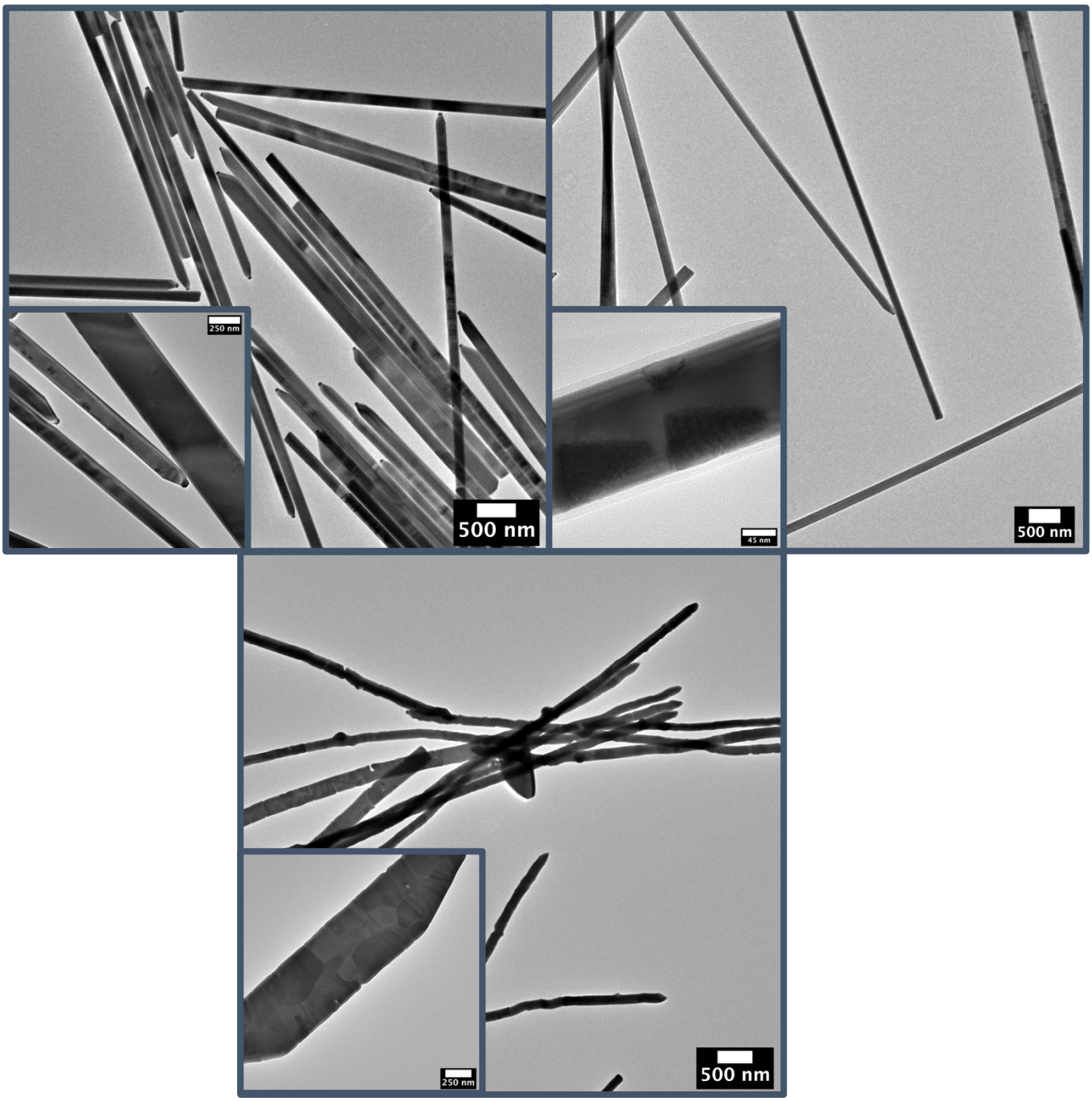

***Figure 4.3**: TEM images. **A.** Nanowires after reaction time of 30 minutes. **B**. Nanowire after reaction for 60 minutes. **C.** Nanowire after 120 minutes of reaction. Inset images, same sample but one or multiple nanostructures magnified*

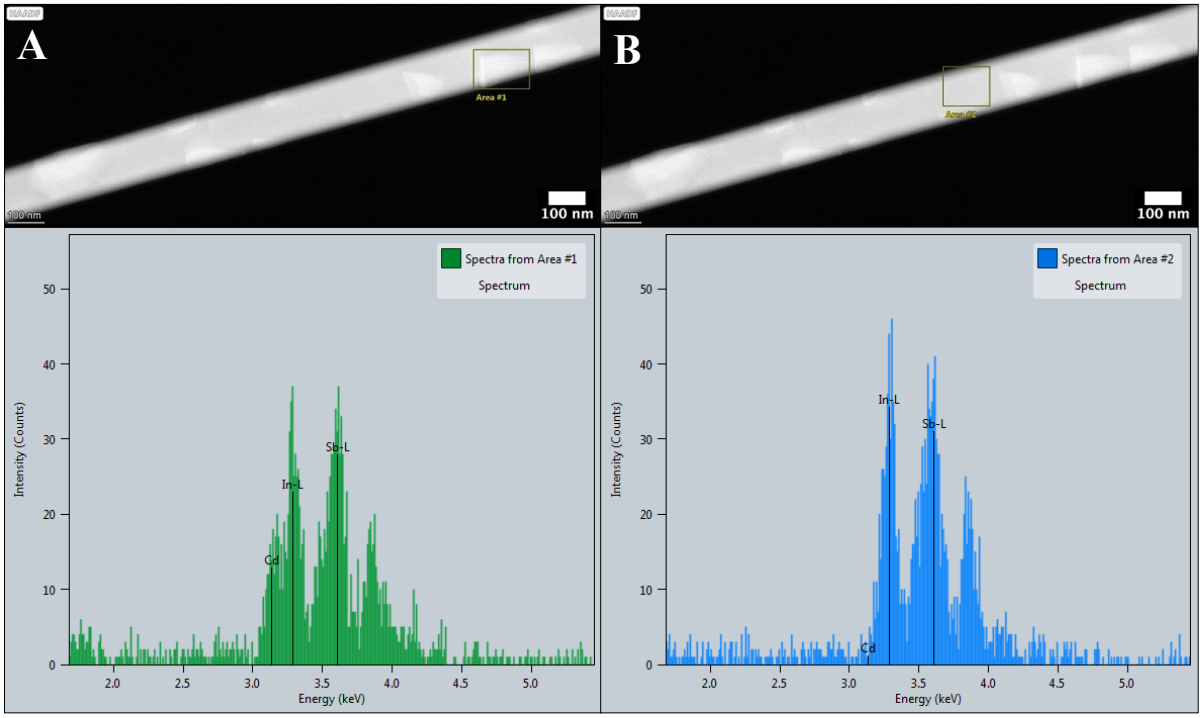

Figure 4.4: HAADF images of a nanowire and the respective EDS analysis of the selected areas. ***A.*** *A transformed triangular domain of the wire, Area #1, including elemental analysis of this section.* ***B.*** *A pristine area of the wire, Area #2, including elemental analysis of this section.*

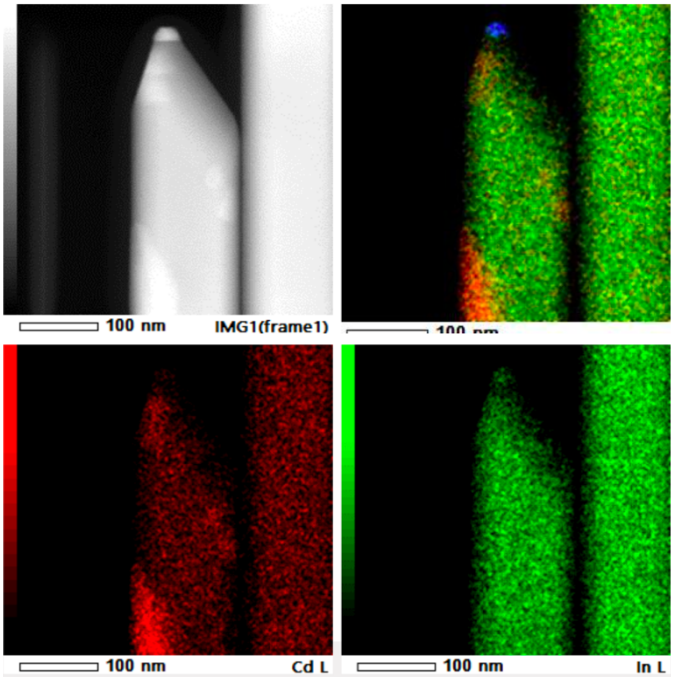

Figure 4.6*: Elemental mapping of partially transformed nanowires, highlighting the cadmium content in red.*

The onset of this In for Cd exchange process appears to be quite stochastic. In Figure 4.5.A, we see an overview of about fourteen nanowires and one nanoflake. At first glance, all the wires look untouched, but upon further inspection, two wires with very few triangular

domains are identified. However, in Figure 4.5.B, we see a nanowire from the same sample, and which is dense with triangular domains. From this, we can infer that the onset of the transformation is rare and stochastic, but once it begins in one wire, it will preferentially continue in said wire.

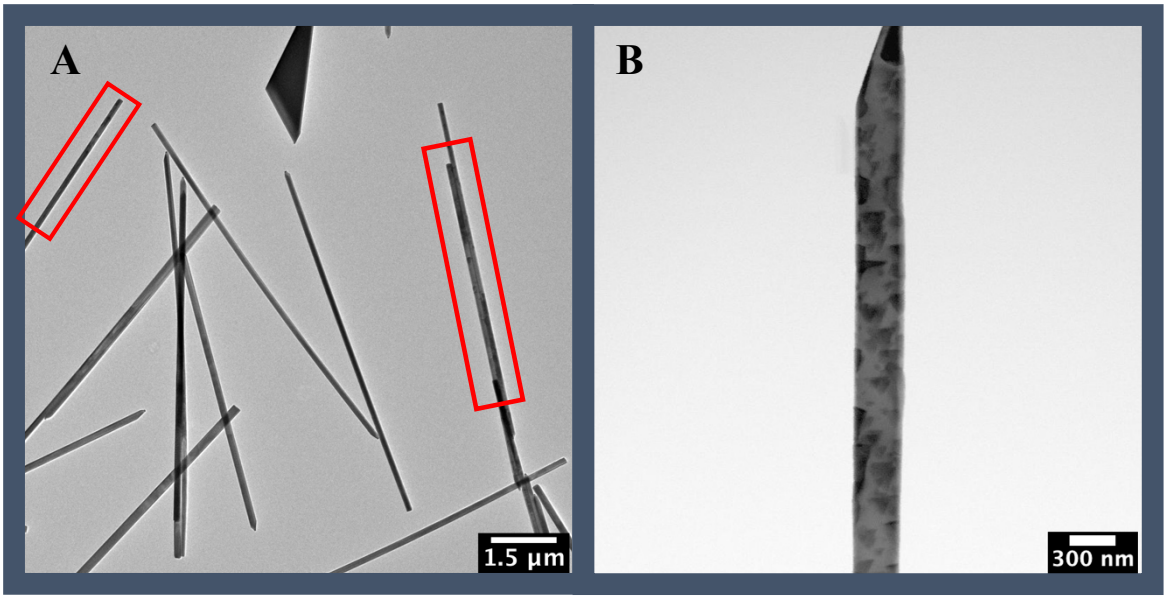

***Figure 4.5**: **A.** TEM image of a collection of wires that appear pristine, with no visible triangular domains of exchange. **B.** Wire from the same sample as the collection in A but showing many triangular domains.*

Finally, although specific reaction times are stated in the analysis above, it is not possible to say that these reaction times are reflective of the reaction rate and that the reaction will proceed at this rate every time the reaction is repeated. This reaction rate can be expected to be limited by solid state diffusion, and thus heavily dependent on the wire diameter. However, it can be concluded that increased reaction times lead to a greater extent of transformation, and a greater number of nanostructures with transformed areas.

The reaction progress was also analysed by SEM to determine whether the whole ensemble could be studied at once. To this end, EDS was carried out on areas such as those shown in Figure 4.1.D-F. This method was found to be useful in that it confirmed that as time progressed, more cadmium was incorporated into the sample, but because the wafers themselves are also InSb, this signal greatly overpowers that of the wires themselves. This imaging was also useful to view the substrate and it allows for some conclusions about the samples. Missing percentages in the following measurements attributed to Si which makes up the mask on the InSb wafer. The Sb/Si ratio is quite constant across all sampled and can be used as an internal standard to show that Sb is not affect by the reaction. For example, a sample reacted for 40 minutes which under TEM measurements showed complete transformation of the thin wires and wedges on thicker wires resulted in SEM EDS data of Cd: 3.7 %, In: 43.0 %, Sb: 47.2 %. These quantities lead to ratios, $\frac{Cd}{In} = 0.088$, $\frac{Sb}{In} = 1.10$, and $\frac{Sb}{Si} = 7.78$. A sample reacted for 60 minutes which under TEM measurements showed complete transformation of the thick and thin wires and wedges on nanoflakes resulted in SEM EDS data of Cd: 3.8 %, In: 43.1 %, Sb: 46.7%. These quantities lead to ratios, $\frac{Cd}{In} = 0.091$, $\frac{Sb}{In} = 1.08$, and $\frac{Sb}{Si} = 7.32$. This data set does not greatly differ from the 40-minute reaction despite the fact that the thick wires

have also fully transformed at this point. Lastly, a sample reacted for 80 minutes which under TEM showed complete transformation of all nanostructures resulted in SEM EDS data of Cd: 20.1 %, In: 29.8 %, Sb: 44.1 %. These quantities lead to ratios, $\frac{Cd}{In}$ = 0.73, $\frac{Sb}{In}$ = 1.52, and $\frac{Sb}{Si}$ = 7.42. These values demonstrate a very large increase in the amount of cadmium, however, due to the substrate itself containing indium, there is a great amount of In remaining. These results help us conclude why it is difficult to assess the reaction progress of an ensemble and why we choose to proceed with conclusions about our reaction based on a collection of imaged and measured nanostructures.

4.3.3 Cd-Oleate concentration

At 180 ºC, the effect of $Cd(oleate)_2$ concentration was investigated. As seen below in Figure 4.7, the wires in each sample reach total conversion after different time periods and the shape of the original wires is preserved. The nanowires reach full conversion after 30, 60 and 80 minutes, at $Cd(oleate)_2$ concentrations of 10^{-1} M, 10^{-2} M and 10^{-3} M, respectively. The elemental composition of these nanostructures in Figure 4.7 are as follows, A. Cd: 58 %, Sb: 42 %, B. Cd: 57 %, Sb: 43 %, and C. Cd: 57 %, Sb: 43 %. From this information, it can be stated that an increase in $Cd(oleate)_2$ concentration results in an accelerated reaction. This dependence is expected because this oleate is the source of the Cd for the reaction. The concentration 10^{-3} M is chosen for the rest of the experiments because the time scale the reaction occurs on allows for the most comprehensive investigation of reaction progress under these conditions.

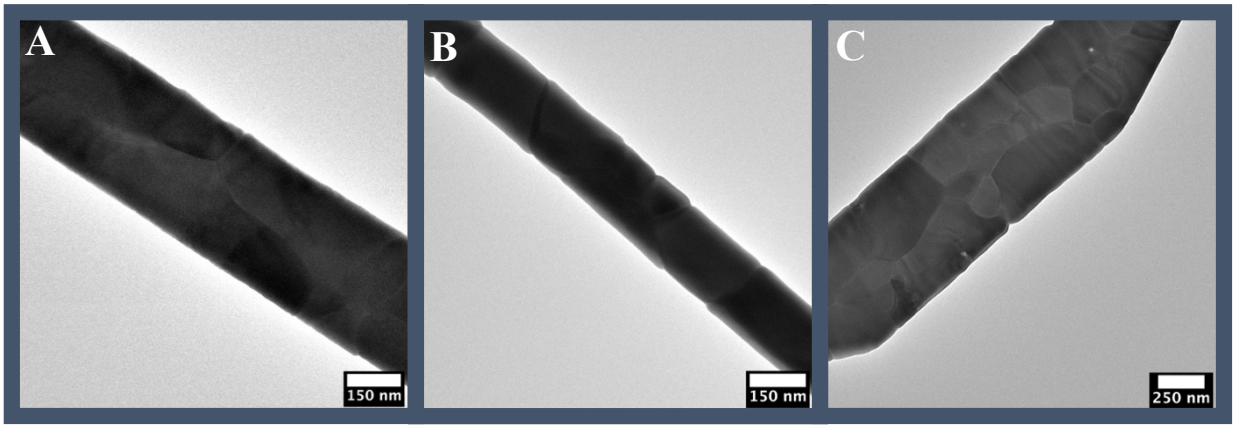

***Figure 4.7**: Completely exchanged nanowires, **A**. 10^{-1}M $Cd(oleate)_2$, and 30 minutes of reaction. **B.** 10^{-2}M $Cd(oleate)_2$, and 60 minutes of reaction. **C.** 10^{-3}M $Cd(oleate)_2$, and 80 minutes of reaction.*

4.3.4 Free oleic acid concentration

The effects of 5 different concentrations of free oleic acid were investigated under reaction conditions of, 180 ºC, 10^{-3} M $Cd(oleate)_2$ and 80 minutes of reaction, The results of these reactions are summarized in Table 4.1. At no excess OA and at $2x10^{-3}$ M, there is no observable changes. At $4x10^{-3}$ M, there is partial transformation visible. At $6x10^{-3}$ M, there is partial transformation visible, with longer segments of the wires transformed. Lastly, at $1x10^{-2}$ M, there is total transformation under these reaction conditions.

Table 4.1: *Table summarizing the extent of transformation at various concentrations of excess oleic acid.*

Oleic Acid Concentration	Extent of Reaction after 80 minutes
0	None
2×10^{-3} M	None
4×10^{-3} M	Partial exchange on terminal segments
6×10^{-3} M	Partial exchange on terminal segments; with longer segments of exchange
10^{-2} M	Complete exchange

Figure 4.8, A and B shows fully transformed wires and a nanoflake, respectively. The composition, determined by EDS, of these fully transformed nanostructures is, Cd: 59.5 %, Sb: 40.4 % and Cd: 57.0 %, Sb: 43.0 % respectively. This composition is Cd:Sb = 1.5, indicating a stoichiometric, but metastable[5,6] elemental composition of Cd_3Sb_2. This composition is unexpected because the thermodynamically stable form is CdSb. The properties of the metastable form are not well studied.

Here, it is worth noting that the extent of exchange in this experiment is qualitatively assessed in a different manner than in the time and Cd(oleate)$_2$ concentration experiments discussed above in sections 4.3.2, and 4.3.3 respectively. In those experiments, samples consisted of wires of diameters between 160 and 350 nm, while the samples used for this set of experiments consisted of wires with diameters between 45 and 75 nm. This is important to note because the wedges that were used as indicators of cation exchange in the afore mentioned experiments were at least 50 nm across at the base of the triangle. Additionally, all of these wedges are dispersed throughout the wire and are oriented towards the gold capped end of the nanowire. This is nearly the whole diameter of the thinner wires. In the thin wires we do not see these wedges, but rather whole sections of exchange, and they all seem to begin at the terminal ends of the wires (not gold capped).

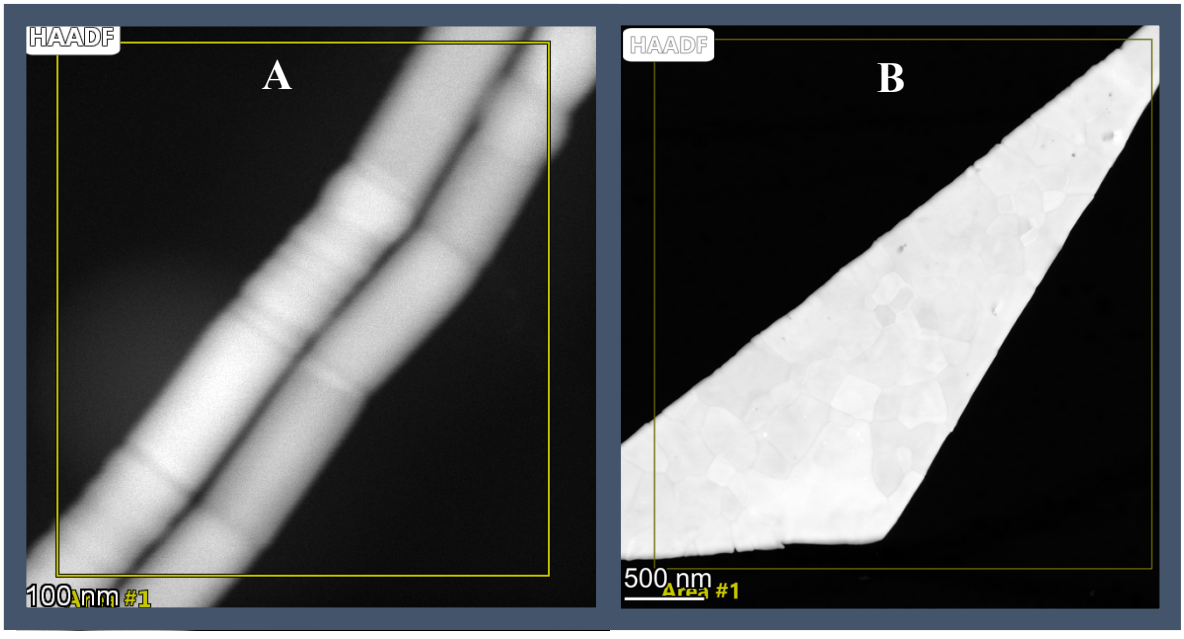

Figure 4.8: *HAADF images of* ***A****. Fully transformed nanowires.* ***B****. Fully transformed nanoflake.*

4.3.5 Crystal structure

There are a few important points that can be deduced about the crystal structure of these transformed nanowires. In Figure 4.10, we see the direction of the lattice preserved in the original material and the transformed portion, this indicates that the antimony sublattice imposes constraints on these wires and limits the structure and resulting composition of the nanowires. For the most part the wires seem to keep their initial diameter and shape, more clearly seen in nanoflakes the exchange proceeds along preferential crystallographic directions of the zinc blende InSb nanowire. Below, in Figure 4.9, the alignment of the wedges in the same direction is shown, and in B, the FFT of the InSb and Cd_3Sb_2 portions respectively, showing that even after exchange, the material remains single crystalline. In addition to this single crystallinity, in Figure 4.10 A and B, we see the electron diffraction patterns for the Cd_3Sb_2 and InSb portions respectively. The alignment of these patterns implies a common crystallographic orientation, and we can conclude that the exchanged portion retains the antimony sublattice of the original material.

A deeper discussion of the crystal structure of the resulting Cd_3Sb_2 nanowires is beyond the scope of this thesis and cannot be resolved with certainty.

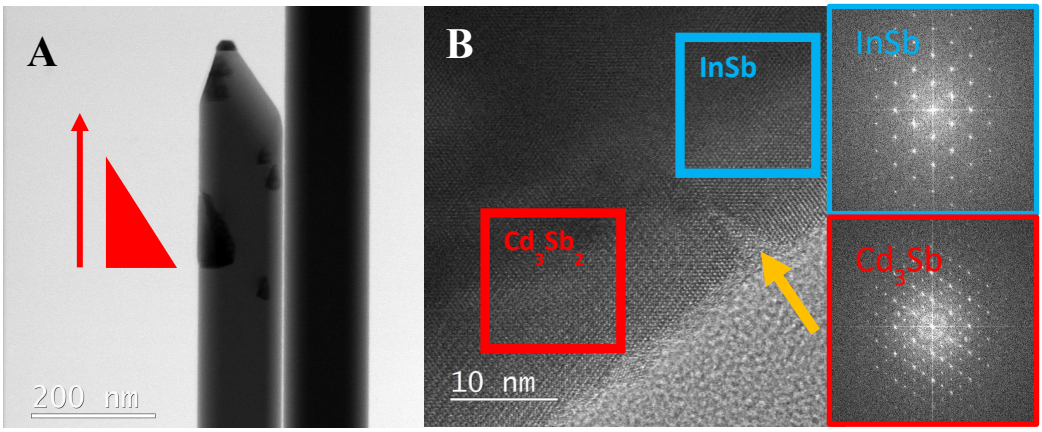

Figure 4.9: *TEM images of **A**. Nanowire with wedges of exchange, **B**. FFT of InSb and Cd3Sb2 portions of partially transformed nanowires*

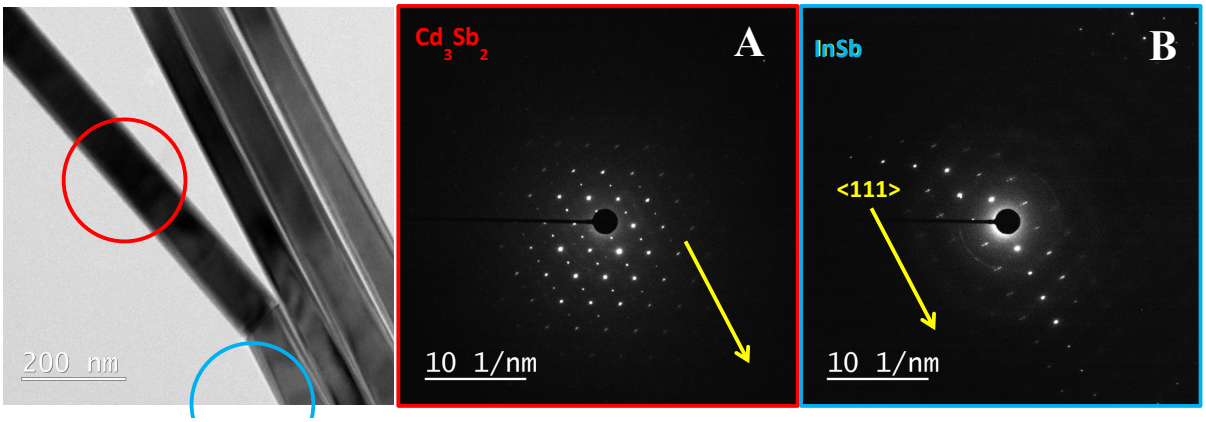

Figure 4.10: *Electron diffraction of **A**. Cd3Sb2 portion of nanowire, **B**. InSb portion of nanowire*

The XRD pattern of a fully transformed sample, Figure 4.11 A and B, shows only two additional peaks that cannot be assigned to zinc blende InSb. The pattern observed matches the distances of the $Cd_{0.57}Sb_{0.43}$ phase peaks, and the extra peaks are seen at ~32 2 Theta degrees and ~66.5 2 degrees theta. These peaks can be assigned to the fully transformed nanowires. Given that the InSb template nanowires were oriented with respect to the InSb substrate, so will the product Cd_3Sb_2 nanowires.

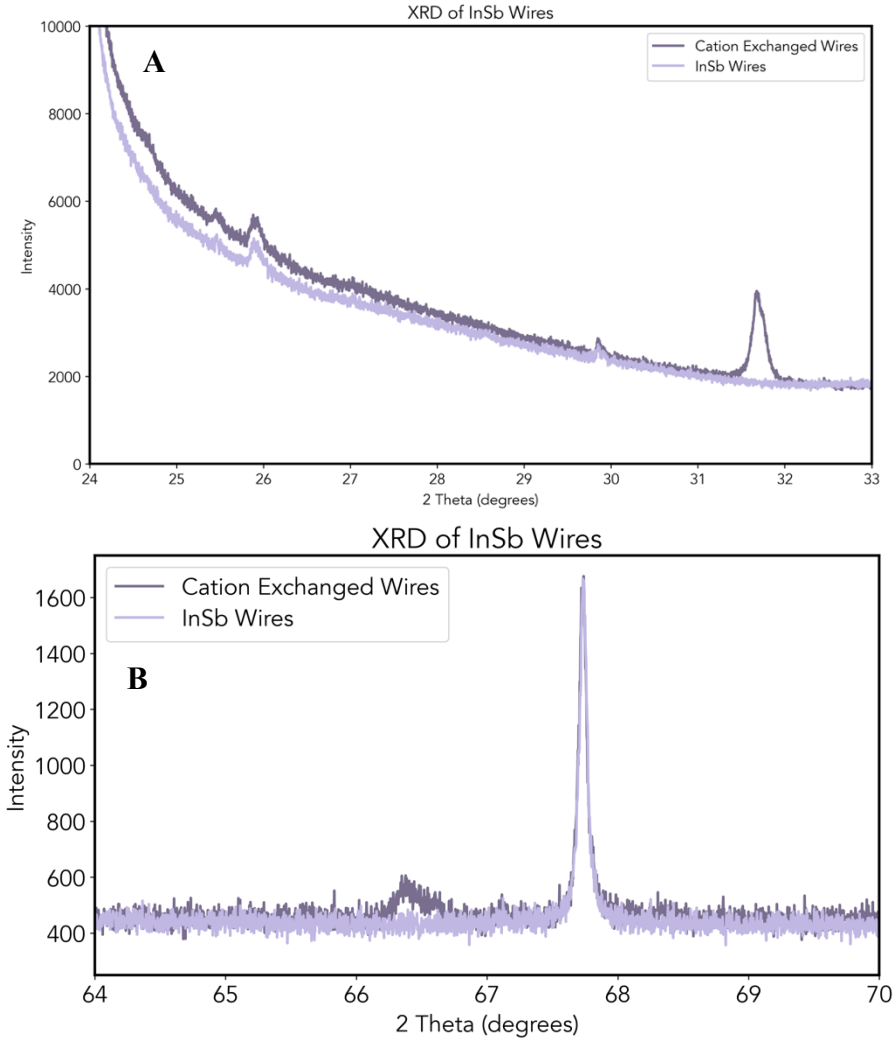

Figure 4.11: *XRD pattern of pristine and cation exchanged nanowires spanning* ***A****. 24-33 2 Theta degrees,* ***B.*** *64-70 2 Theta (degrees)*

4.3.6 Reaction with other metal oleates

The interesting results that we saw with $Cd(oleate)_3$ led us to test the reaction with various metal oleates. In an example using 10^{-3} M $Bi(oleate)_3$, and 30 minutes reaction time, progress depicted in Figure 4.7, it is quite clear that the mechanism in this reaction is significantly different. At 60 °C, Figure 4.7.A, wires remain pristine. At 70 °C, Figure 4.7.B, some reaction seems to take place at the surface. As the temperature is raised to 75 °C, Figure 4.7.C, this reaction is more evident. Lastly, at 100 °C, the wire is completely deformed as it adopts a stacked rhombohedral shape. In addition to the elemental analysis in Figure 4.8, of

this wire, we see that the result of this reaction is complete Bi for In and Sb exchange. The activation energy for this reaction is also much lower than the 180 °C required for the Cd for In exchange. Unlike the wedge progress in the Cd for In exchange, here the reaction appears to corrode the wires. This corrosion can be rationalized by galvanic replacement, where the bismuth oxidizes both indium and antimony. Upon reflection, the results of this experiment, such as the lowered activation energy and the fact that there is total exchange is something that could be predicted by the reduction potentials of each metal involved. Bismuth has a reduction potential of 0.308 eV, cadmium, -0.402 eV, antimony, -0.510 eV, and indium, -0.444 eV.[8] The reduction potential of bismuth is much higher than that of both indium and antimony, so it proceeds with replacing both in the structure. The galvanic replacement process dominates this reaction and goes to completion. In the case of cadmium exchange, the reduction potential is only slightly higher, so the process requires more energy input to proceed, and is also balanced by a cation exchange where it only replaces the indium in the structure.

Additionally, when this experiment is carried out with Zn(oleate) or Cu(oleate), no such exchange, partial or complete takes place. Again, referring to reduction potentials, zinc has -0.762 eV and copper, -0.339 eV,[8] so no galvanic replacement reaction is expected at all.

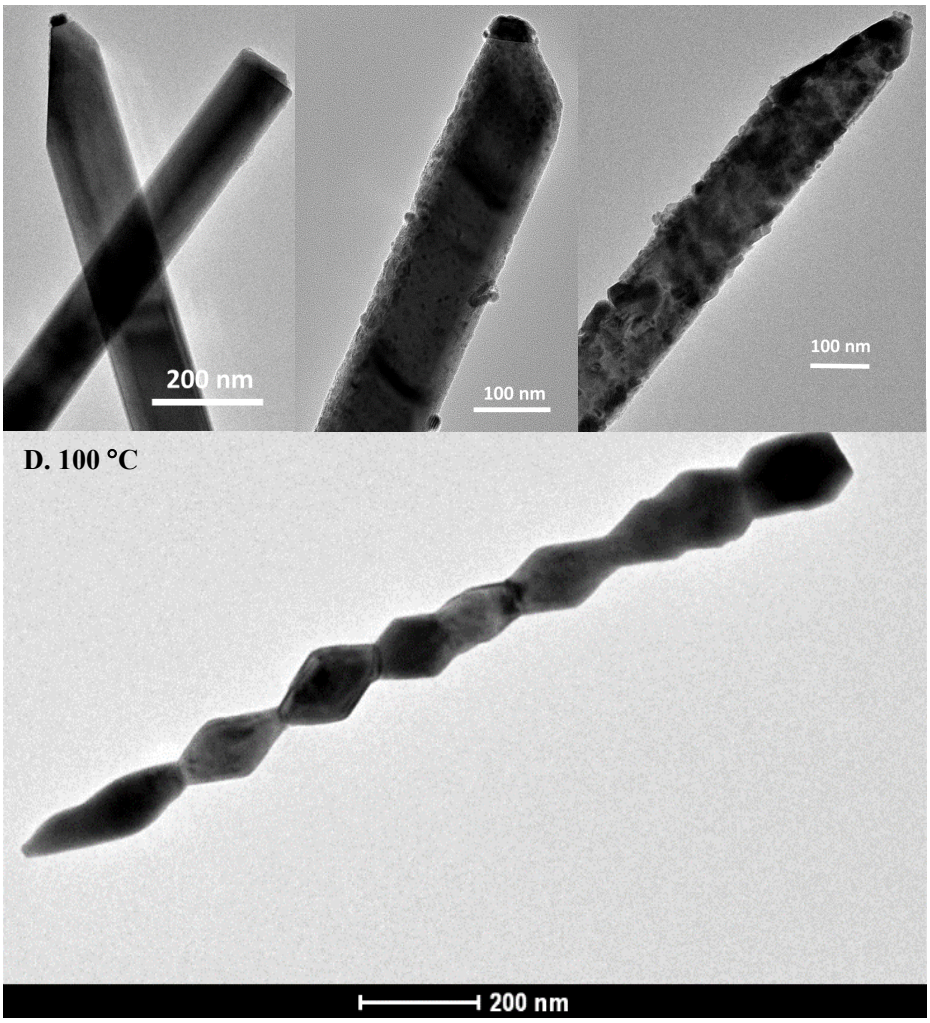

Figure 4.12: *TEM images of InSb nanowires reacted with 10^{-3} M $Bi(oleate)_3$ for 30 minutes at* ***A.*** *60°C,* ***B.*** *70°C,* ***C.*** *75°C, and* ***D.*** *100°C,*

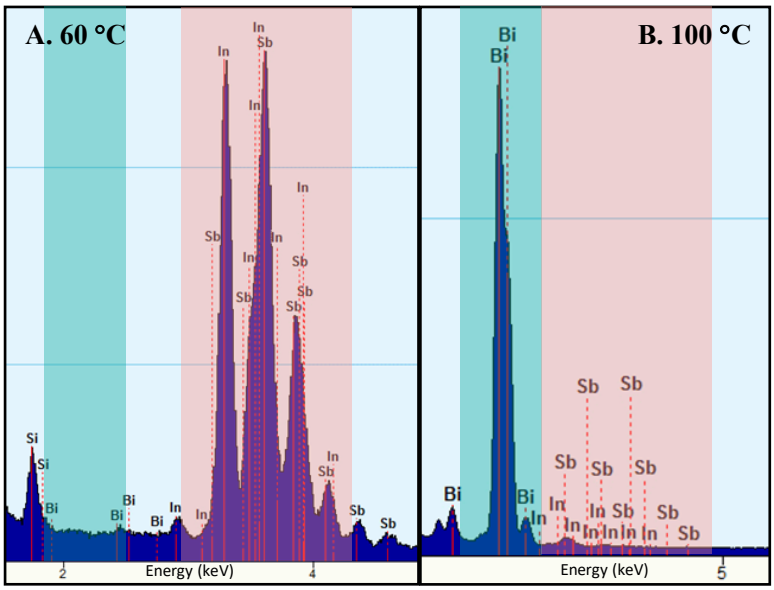

Figure 4.13: *Elemental composition of InSb wires reacted with 10^{-3} M Bi(oleate)$_3$ for 30 minutes at **A.** 60°C, and **B.** 100°C.*

4.3.7 Proposed mechanism

From the discussion above, we can conclude that Cd for In metal exchange takes place in this reaction. We determined that the reaction requires an excess of OA to proceed, and as the concentration of the excess increases, the reaction rate increases. We propose that this excess is required because of the charge difference between Cd^{2+} and In^{3+}. In Cd(oleate)$_2$ the cadmium is bound to only two oleate molecules (Figure 4.14.A), but to preserve the charge balance when the direct exchange between In^{3+} and Cd^{2+} takes place, the In^{3+} requires a third oleate molecule (Figure 4.14.B). This then supports the statement that an increased concentration of free OA increases the reaction rate. Effectively, if there is a greater amount of free oleate molecules available, they are able to stabilize more leaving In^{3+} from the wires in the solution, increasing the rate of reaction. When the first indium is replaced by cadmium, there is an exchange of electrons, and this excess electron is localized around the antimony remaining in the wire (Figure 4.14.C). This charge imbalance causes a runaway chain or diffusion flux of Cd for In, penetrating the depth of the wire to try to achieve neutrality (Figure 4.14.D). Due to the high electron mobility of InSb,[1] this spare electron can move along the surface of the wire, and potentially pose as the site of the next "attack" point for a Cd(oleate)$_2$ complex to adhere to (Figure 4.14.E). This flux results in the Cd:In = 1.5, which is consistent with Cd_3Sb_2, which although metastable, is the form that is required in this structure to maintain electron neutrality and wire shape. This reaction must self-propagate to maintain charge balances, so it continues in one wire while some nanowires remain untouched.

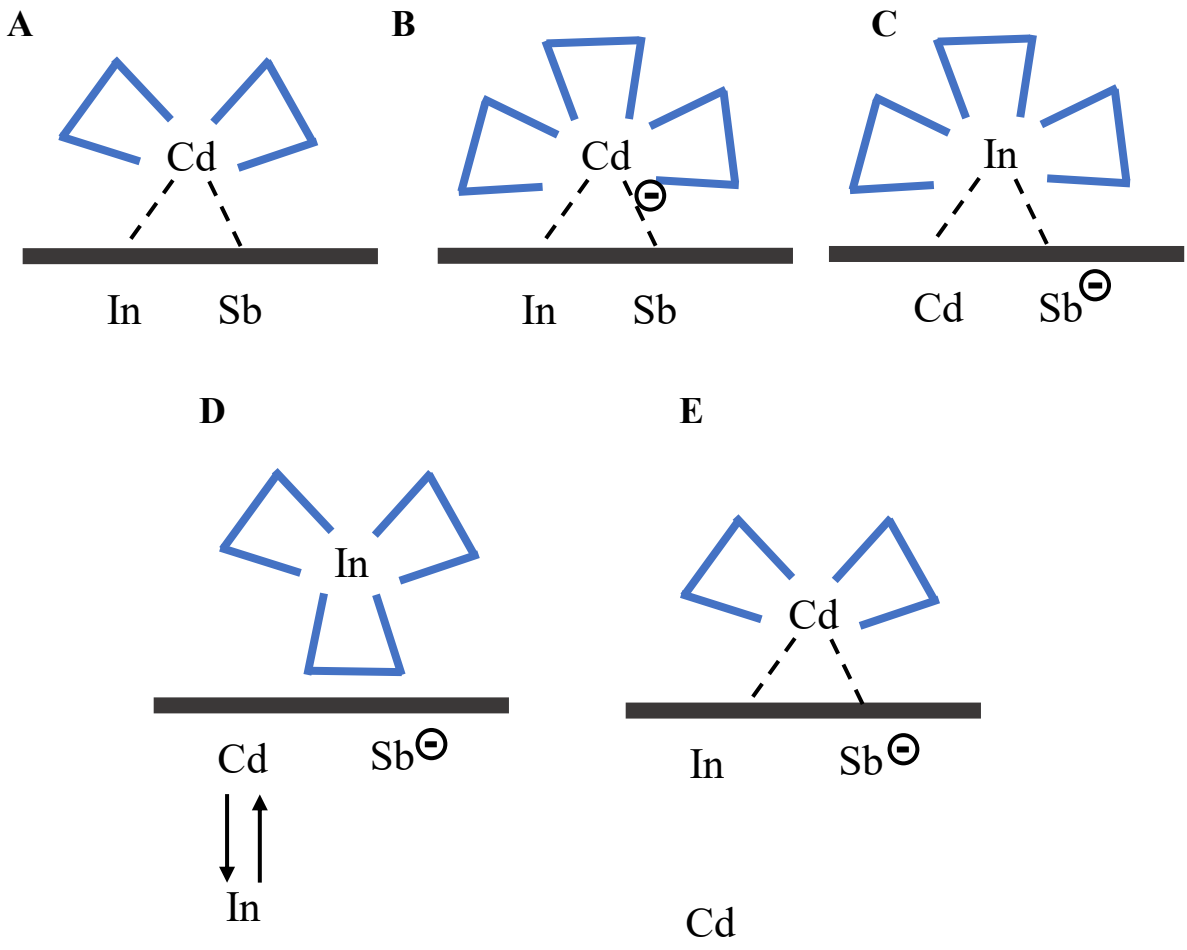

Figure 4.14: *Schematic representation of proposed mechanism of exchange.* ***A.*** *Approach of $Cd(oleate)_2$ complex to InSb wire surface.* ***B.*** *Complexing of a third oleate molecule $Cd(oleate)_2$ bound to the InSb nanostructure surface.* ***C.*** *Swap of indium and cadmium.* ***D.*** *Release of $In(oleate)_3$ complex from surface into solution, as cadmium penetrates through the depth of the wire to correct the charge imbalance.* ***E.*** *Attachment of another $Cd(oleate)_3$ complex on the surface of the nanowire where there is a charge imbalance left over from the last swap.*

4.4 Conclusion and outlook

It can be concluded that the system of transformation of InSb nanowires to Cb_3Sb_2 is a fine balance of cation exchange and galvanic replacement. We cannot define reaction times and rates with confidence, but we can safely conclude that under the conditions we have defined, increased reaction times lead to greater amounts of transformation in all nanostructures in a sample. This reaction requires an excess of free oleic acid in solution to proceed because of the charge difference between Cd^{2+} and In^{3+}. The onset of the reaction is stochastic, but once it begins, it will likely proceed to completion before beginning in a different nanowire or flake because the onset of the reaction creates a charge imbalance in the nanostructure, that leads to a self-propagating process. The reaction does not proceed in the same manner in experiments with bismuth, zinc, and copper oleates. When reacted with $Bi(oleate)_3$ at a lower temperature, galvanic replacement dominates, where both indium and antimony are completely replaced, and the wire adopts a stacked rhombohedral structure. With zinc and copper oleates, the reaction does not proceed at all.

To further understand the mechanism and reaction rates of this system, it would be beneficial to design an in-situ experiment that would allow for elemental analysis during the progress of reaction and for the whole ensemble to be studied. An in-situ analysis would allow for determination if there is any hinderance to the reaction due to wire spacing, and it would allow for many wire diameters to be investigated simultaneously.

4.5 References

[1] Badawy, G., et al. High Mobility Stemless InSb Nanowires. *Nano Lett.* 19, 3575-3582, (2019).

[2] Park, H. D., et al. Growth of high quality, epitaxial InSb nanowires. *J. Cryst. Growth.* 304, 2, 399-401, (2007).

[3] van Weperen, I., et al. Quantized Conductance in an InSb Nanowire, *Nano Lett.* 13, 2, 387–391, (2013)

[4] wang, S., et al. Anisotropic Multicenter Bonding and High Thermoelectric Performance in Electron-Poor CdSb. *Chem. Mater.* 27, 3, 1071–1081, (2015).

[5] R. Garcia-Rodriguez, H. Liu, Solution Structure Of Cadmium Carboxylate And Its Implications For The Synthesis Of Cadmium Chalcogenide Nanocrystals. *Chem. Commun.* 49, 7857, (2013)

[6] Seltz, H., DeWitt, B.J. A Thermodynamic Study of the Cadmium-Antimony System. *J. Am. Chem. Soc.* 60(6), 1305-1308, (1938).

[7] Zabdyr, L.A., Equilibrium Diagram and Thermodynamic Properties of Cadmium-Antimony Binary Alloys. Critical Assessment. *CALPHAD.* 17(2), 125-132, (1993).

[8] Harris, D. C. (2010). *Quantitative Chemical Analysis, 8th Edition*. W.H. Freeman.

6. Acknowledgements

To Celso de Mello Donegá, thank you so much for taking a chance on me and believing in me and my abilities enough to entrust me with two projects. I thank you for your trust in me, kindness, patience, and guidance through this project. To Serena, thank you for taking me under your wing and teaching me the ins and outs of our glovebox and the great company and friendship. To Raimon, thank you for taking me on as an extra student to pick up a project at the last minute. I appreciate your trust in me and my independence in the lab. Gru's lab will be greatly missed. To the team in Eindhoven, Ghada, Eric, and Marcel, thank you for providing samples, constructive conversations in meetings, and doing additional excellent extra TEM measurements for us. To Maaike and Jara many thanks for always being there to answer all of my silly lab questions and chats.

A special thank you to my parents for the endless support and love I have received throughout my whole life. While my choice to leave Canada for grad school was drastic, coming to the Netherlands was always my dream, and I wouldn't have been able to do any of it without the two of them, their support and undying belief in me, it means A LOT. I am so lucky to have such wonderful, caring parents. To my family in the Netherlands for taking me in and making me feel at home, I am eternally grateful.

To my friends, near and far, thank you for being incredible cheerleaders. Finally, to all of the master students, thank you for the jokes, the memes, the coffee breaks, the never-ending games of kaboo, and the emotional support throughout the past year.

7. Appendices

7.1 Appendix 1

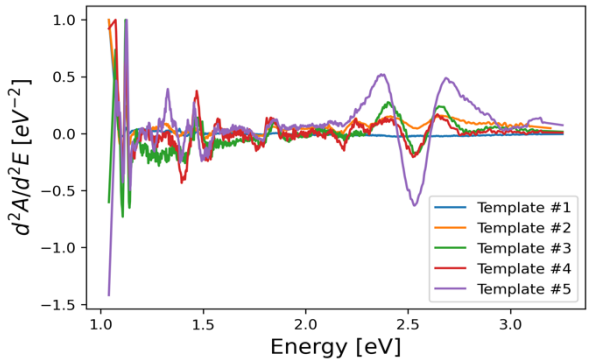

***Figure A1.1**: Plots of second derivative of absorbance spectra shown in Figure 3.1 in the main text. Minima used to calculate the exact location of the shoulder around 500 nm*

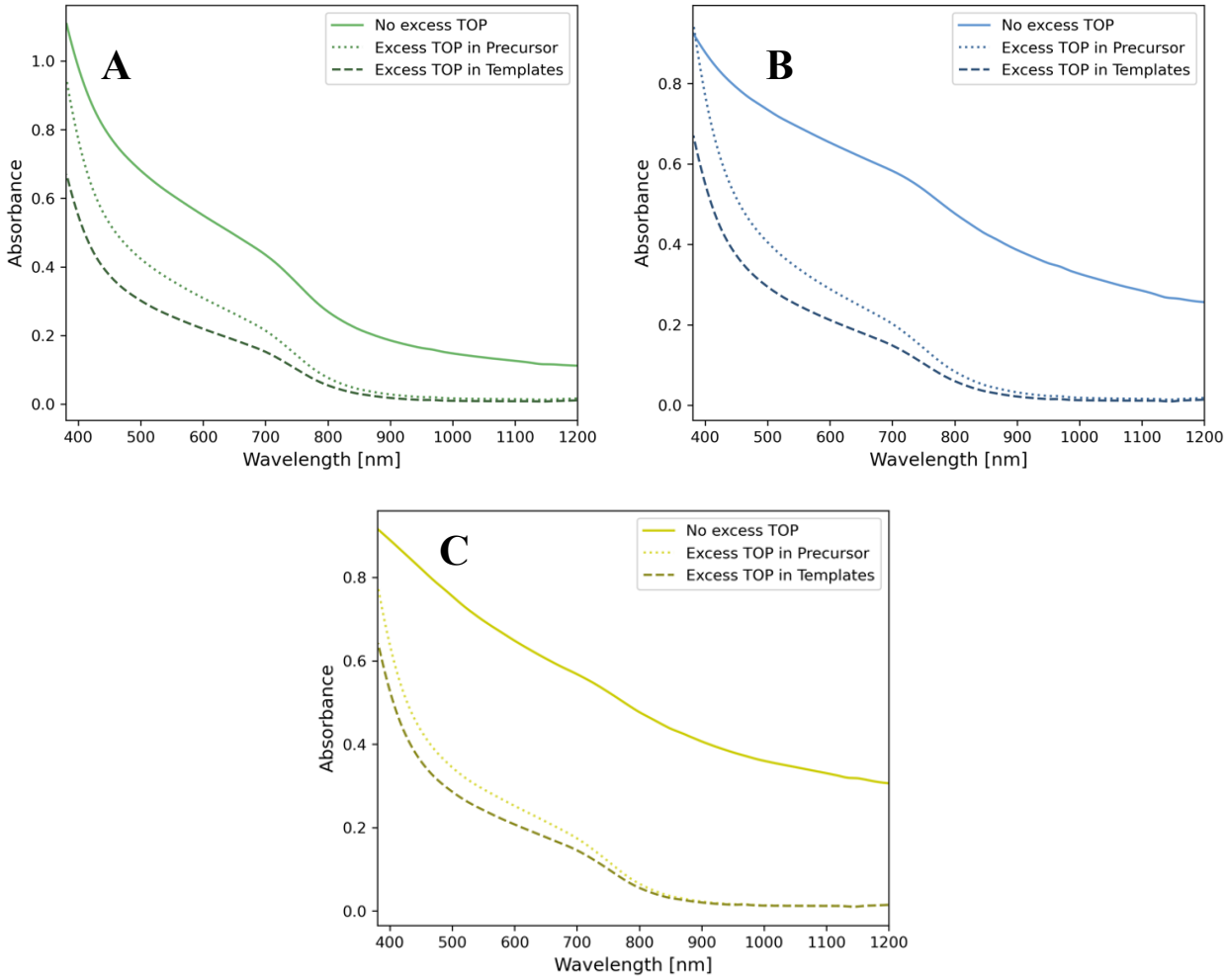

***Figure A1.2:** Un-normalized absorbance spectra of sets of reactions carried out with Template #4. Sets includes a control, with no excess TOP, and 2 reactions with 50 µL excess TOP each, one in the precursor and one in the template. Template exposed to excess TOP for 3 minutes. **A.** Set of reactions carried out with In/Cu = 4.0. **B.** Set of reactions carried out with In/Cu = 2.0. **C.** Set of reactions carried out with In/Cu = 1.0.*

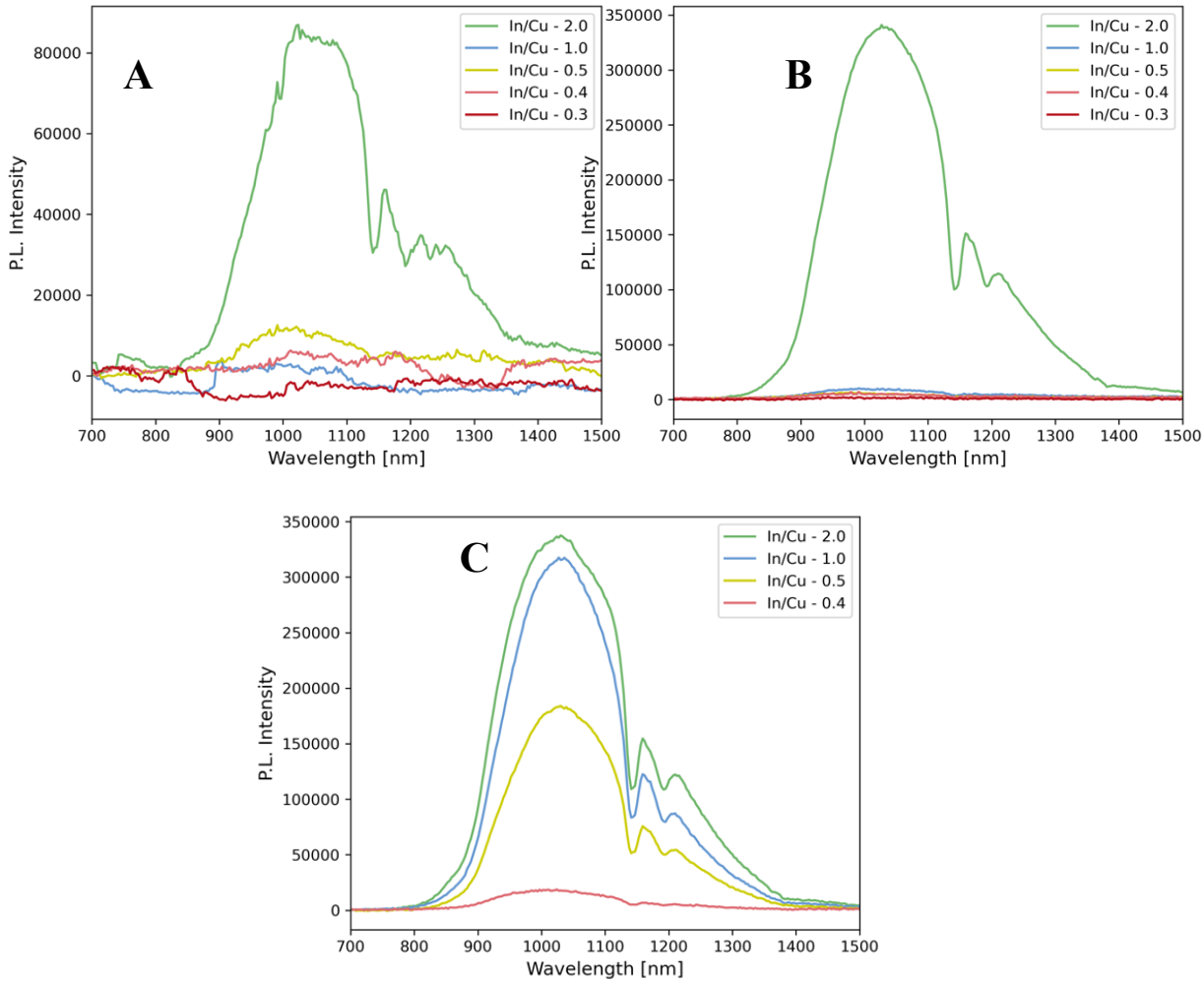

Figure A1.3: *Un-normalized emission spectra of three sets of cation exchanges carried out with Template RT11, using washing method D, as previously defined.* ***A.*** *Spectra of control set of experiments, cation exchange with no excess TOP addition. TOP/In ratio 1:1 in all cases.* ***B.*** *Spectra of set of experiments with 16 µmol excess TOP added to the $InCl_3$ precursor. TOP/In ratios of 1.36, 1.73, 2.45, 2.78 and 3.29 corresponding respectively to the In/Cu ratios of 2.0, 1.0, 0.5, 0.4, 0.3.* ***C.*** *Spectra of set of experiments with 47 µmol excess TOP added to the $InCl_3$ precursor. TOP/In ratios are as follows, 2.06, 3.14, 5.27, 6.22, corresponding respectively to the In/Cu ratios of 2.0, 1.0, 0.5, 0.4.*

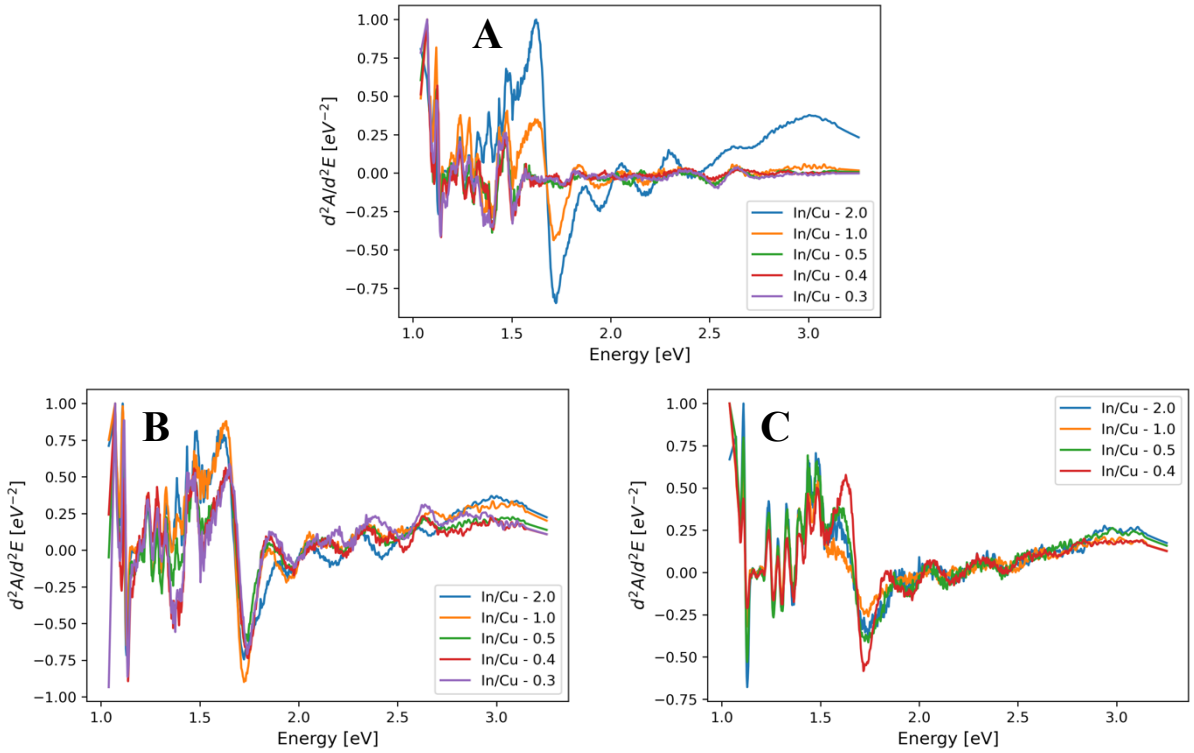

Figure A1.4: *Plots of second derivative of absorbance spectra shown in Figure 3.10 A, C and E in the main text. Minima used to calculate the location of the band-edge transition.*

Table A1.1: Summary of reactants used in cation exchange reactions whose optical measurements are shown in Figure 3.10 of the main text.

Sample Name	Volume of template used (mL)	Cu (mmol) in templates	Amount of indium precursor (mL)	Amount of excess TOP (µL)	In (mmol) in precursor	Extra ODE (mL)
KCCE 2-17	0.431	0.044	0.444	0	0.044	2.125
KCCE 2-18	0.431	0.044	0.222	0	0.022	2.347
KCCE 2-19	0.431	0.044	0.111	0	0.011	2.458
KCCE 2-20	0.431	0.044	0.089	0	0.009	2.480
KCCE 2-21	0.431	0.044	0.067	0	0.007	2.503
KCCE 2-22	0.431	0.044	0.444	16	0.044	2.125
KCCE 2-23	0.431	0.044	0.222	16	0.022	2.347
KCCE 2-24	0.431	0.044	0.111	16	0.011	2.458
KCCE 2-25	0.431	0.044	0.089	16	0.009	2.480
KCCE 2-26	0.431	0.044	0.067	16	0.007	2.503
KCCE 2-27	0.431	0.044	0.444	47	0.044	2.125
KCCE 2-28	0.431	0.044	0.222	47	0.022	2.347
KCCE 2-29	0.431	0.044	0.111	47	0.011	2.458
KCCE 2-30	0.431	0.044	0.089	47	0.009	2.480

Table A1.2: Gallium Precursors Compositions

Precursor	Amount of Ligand	Amount of $GaCl_3$	Amount of Toluene
I	0.504 g (DDT)	0.439 g	4.402 mL
II	0.508 g (DDT)	0.441 g	4.402 mL
III	0.468 g (DPP)	0.439 g	4.565 mL

7.2 Appendix 2

7.2.1 Experimental: Trioctylphosphine treatment of InSb nanowire wafers

To carry out what is referred to as a "TOP treatment", an InSb wafer is submerged in 1 mL of TOP, enough to completely cover the bottom of the vial. The wafers are left submerged in this TOP for one hour and then the liquid is removed by micropipette. To wash away the remnants of the TOP, the wafers are then washed first with 5 mL toluene and then with 2.5 mL of toluene. The vial is then left uncovered in the glovebox to evaporate the rest of the toluene before the wafers are used for cation exchange.

7.2.2 Discussion: Trioctylphosphine treatment of InSb nanowire wafers

Upon original experiments, TOP treatment of the nanowire wafers was thought to be required, however, upon direct comparison to untreated samples, this TOP treatment was determined to be inhibiting the Cd for In exchange reaction, evidence of this is shown below in Figure A2.1. The original intent of the TOP treatment was to react with any oxide at the surface and clean the surface because of InSb's extreme propensity to oxidize. However, due to the lack of certainty in the initiation of the reaction, perhaps the cation exchange begins at an imperfection on the wire that is removed upon the treatment of the wafer with TOP, inhibiting the onset of the cation exchange. Thus, all subsequent reactions were carried out without TOP treatment of the wafers.

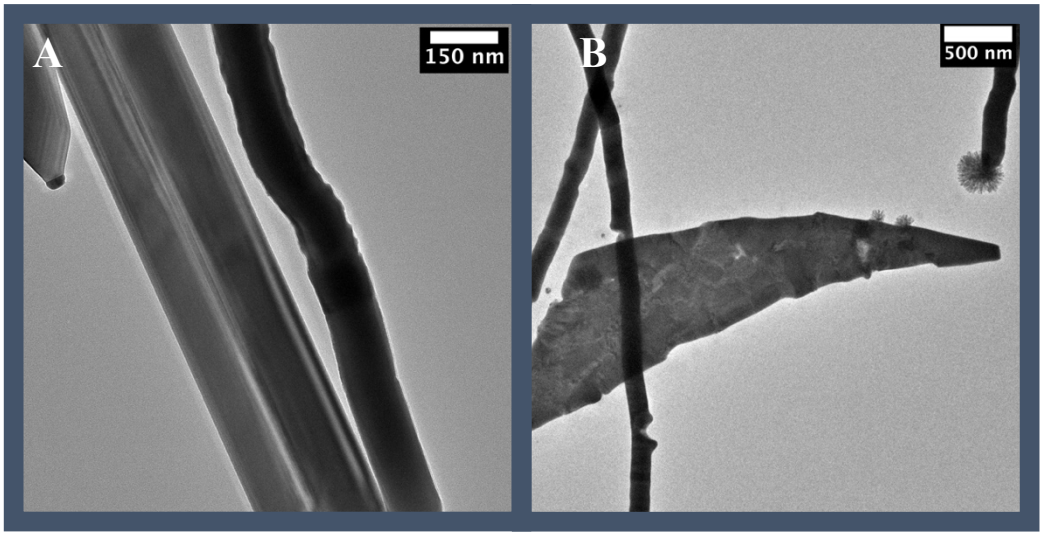

Figure A2.1 ***A.*** *Wires from an exchange reaction on a TOP treated InSb wafer, after 90 minutes of reaction.* ***B.*** *Wires and flake from an exchange reaction on an untreated InSb wafer, after 90 minutes of reaction.*